Growth, Phase Transition, and Island Motion of Au on Ge(111)

J. A. Giacomo¹, C. H. Mullet,² and S. Chiang³

Department of Physics University of California, Davis

1 Shields Avenue

Davis, California 95616-5270, USA

Abstract

Using low energy electron microscopy (LEEM), Au on Ge(111) is determined to follow a

Stranski-Krastanov growth mode consisting of a single layer up to 1 monolayer (ML), followed

by 3-dimensional Au-Ge alloy droplets. Near 600°C, we report the first observation of a

reversible first-order phase transition that occurs from the $(\sqrt{3}x\sqrt{3})R30^{\circ}$ phase to a (1x1) phase,

which has coverage of 0.367ML. The transition occurs gradually through a coexistence region

with a temperature range of about 2°C and weakly depends on coverage, varying from 640°C at

1ML down to 580°C at 0.8ML. The phase transition is accompanied by phase fluctuations of

small domains or the fluctuations of phase boundaries of large domains. At coverage >1ML and

above 250°C, the 3D droplets move with stick-slip hopping behavior that has been previously

explained by dissolution of Ge at step edges into the alloy droplet, which then comes to

concentration and thermal equilibrium via the island motion.

Keywords: Au; Germanium; Low Energy Electron Microscopy; Surface Structural Phase

Transition: Phase Fluctuations

¹ Present address: Air Quality Research Center, University of California Davis, Davis, CA

95616-5270

² Present address: Intel Corporation, Hillsboro, OR, 97124

³ Corresponding author: chiang@physics.ucdavis.edu

1

1. Introduction

As a typical metal on semiconductor system, Au/Ge(111) is part of a group of similar systems such as Ag, Sn, Pb, and Ni on elemental semiconductor surfaces. These systems enjoy a long history of exploration by many different surface science techniques as they have intrinsic technical and fundamental importance. As the age of semiconductor transistors and electronics has boomed, the value of understanding the nature of metal semiconductor interactions at surfaces has also. The smaller we continue to shrink our electronics, the more impact our understanding of surface interactions will have on further technological advancement. Beyond the technical implications, there is also fundamental knowledge to be gained. Many new surface science techniques have used systems such as these as prototypes to explore new physics.

The noble metal on elemental semiconductor systems have been well studied. In particular, it is intriguing to note that in all four systems, Au and Ag on Ge(111) and Si(111), there is a $(\sqrt{3}x\sqrt{3})R30^{\circ}$ (abbreviated as $\sqrt{3}$ in the following discussions) phase. The structure of these $\sqrt{3}$ phases has been probed by techniques such as scanning tunneling microscopy (STM),^{2, 12-17} low energy electron diffraction (LEED),³ surface x-ray diffraction (SXRD),^{4, 9, 18} and angle-resolved photoemission spectroscopy (ARPES).¹⁹ These structures have been compared and an interesting relationship was found. Ag/Si(111) and Ag/Ge(111) both share a honeycomb chained trimer (HCT)^{4, 20-23} structure while Au/Si(111) and Au/Ge(111) share a conjugate honeycomb chained trimer (CHCT) structure.^{9, 24, 25} Of the four systems, although Au/Ge(111) has the simplest phase diagram, it has received the least attention.⁵ This paper describes low energy electron microscopy (LEEM) and low energy electron diffraction (LEED) studies of this system, including the dynamics of the $\sqrt{3}$ phase during growth, the $\sqrt{3}$ to (1x1) phase transition, and movement of Au-Ge alloy droplets that form for coverage >1monolayer (ML, defined as the

atomic density of the unreconstructed Ge(111) surface, $7.22x10^6$ atoms/ μm^2). LEEM is a powerful technique for studying these phenomena because of the combination of real-time data acquisition, including movies showing sample dynamics, and the ability to dose and heat during image acquisition. We also show one set of STM and LEEM images of the same sample, illustrating the complementary data obtained by the two techniques.

2. Experimental Methods

The experiments were performed in an ultrahigh vacuum (UHV) system consisting of three connected chambers housing several commercial instruments, including LEEM (Elmitec GmbH), STM (Oxford Instruments), and x-ray photoemission spectrometer (XPS, Vacuum Generators). ²⁶ Ge(111) samples of 5 x 5 mm² were cut from 2 inch wafers of n-doped germanium (MTI Crystal), with resistivity ~0.25 ohm-cm and polished on one side with miscut <0.5°. The LEEM sample holder has an integrated tungsten filament to allow electron beam heating of the sample during data acquisition. The sample temperature was measured with a K-type thermocouple in contact with the back edge of the sample, which was calibrated with an infrared pyrometer. The Ge(111) surface was cleaned by repeated Ar⁺ ion bombardment at 500eV and annealing at 800°C until a sharp Ge(111) c(2x8) LEED pattern was observed. The thermocouple calibration was checked by measuring the temperature of the Ge(111) c(2x8) to (2x1) phase transition, which was found by Phaneuf and Webb to occur at 300°C. ²⁷ The temperature controller could hold the sample temperature constant within a range of 2°C.

Au was dosed from a hot filament evaporator consisting of Au wire wrapped around a tungsten filament that was heated by passing current through it. The evaporator was mounted onto the LEEM sample chamber and dosing was done during imaging so that growth phenomena could be directly observed. Calibration of the Au dosing was done by assuming the saturation coverage

of Ge(111)- Au $\sqrt{3}$ to be 1.0ML, as agreed upon in the literature. By analyzing the LEEM images, the dosing rate at the evaporator current of 7.50 A was found to be 0.14 ML/min. The same value of Au flux was used for all data shown in this paper with varying Au coverage (Figs. 3, 4, 15, 16, and 17.)

3. Experimental Results and Discussion

3.1. Phase Diagram of Au on Ge(111)

The Au/Ge(111) system has a simple phase diagram (Fig. 1), as determined from our LEEM and LEED measurements. LEEM is sensitive to the diffraction caused by structures on the surface but not to details of the atomic structure. Although LEEM cannot confirm any of the structural models proposed for the $\sqrt{3}$ phase discussed above, it allows real-space imaging of 2D structures on the surface as a function of time, allowing us to understand how Au grows on the surface during deposition.

The Au/Ge(111) system follows the Stranski-Krastanov growth mode, with a single layer of Au forming on the surface, followed by the growth of 3-Dimensional (3D) islands. For deposition temperatures below ~200°C, Au remains on the surface in a disordered arrangement as deposited, with no LEED patterns or LEEM contrast changes. At these lower temperatures, there is not enough energy for appreciable mass movement of the Au adatoms, which therefore stay in their initial adsorption sites, producing no diffraction pattern.

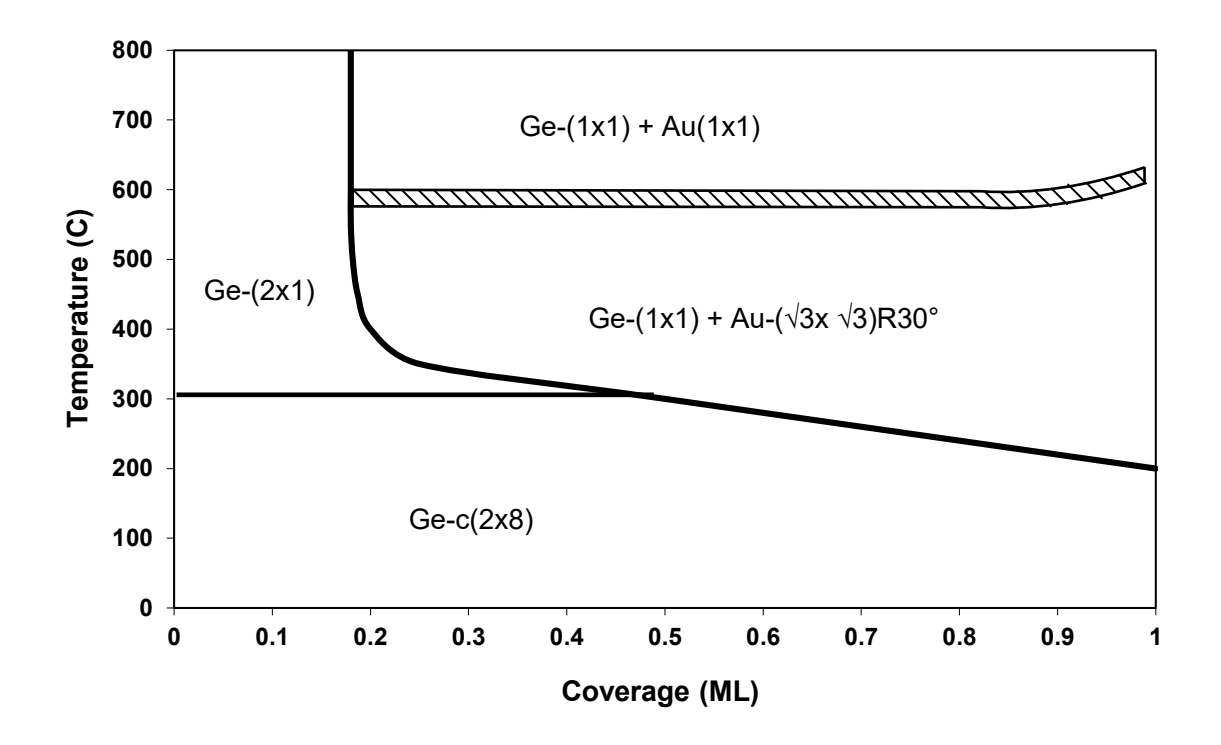


Fig. 1. Au/Ge(111) phase diagram. The hashed section between the Au-($\sqrt{3}x\sqrt{3}$)R30° and Au-(1x1) areas represents a range of temperatures over which the phase transition occurs. Smaller domains undergo the $\sqrt{3}\leftrightarrow(1x1)$ transition at lower temperatures than do larger domains. This effect is explained in more detail in Section 3.2

Very low coverage of Au, ~0.07ML, causes the Ge(111) c(2x8) reconstruction to transform to an incommensurate I(2x2) structure at room temperature, ¹⁰ which is very similar to the high temperature incommensurate Ge(111) phase, observed above 300°C. For clean Ge(111) this phase was previously described by a detailed LEED study as either three orientations of (2x1) structures with quasiperiodic antiphase walls or a (2x2) reconstruction modulated by a honeycomb arrangement of intersecting antiphase walls. ²⁷ The (2x2) structures were observed in a more recent STM and ARPES study, which showed that the $\sqrt{3}$ structure can coexist with the c(2x8) and (2x2) Ge structures. ²⁸ Our limited STM experiments, however, did not resolve clearly

the Ge (2x2) structures induced by small Au coverage. As indicated on the phase diagram in Fig. 1, however, we did observe the high temperature Ge(111) (2x1) pattern using LEED.

When annealed or deposited above 200°C - 350°C (depending on coverage), Au forms the $\sqrt{3}$ structure, which has been identified as a CHCT model, consisting of a metal trimer in a missing top layer structure, as described above. Although Au/Si(111) shares this structure, STM data show that the empty state image produces a honeycomb pattern similar to that of Si(111)- $\sqrt{3}$ Ag, indicating subtle differences of the CHCT structures for Au on Si(111) and Ge(111). Despite disagreement for other noble metal-elemental semiconductor systems, both LEED and SXRD experiments have confirmed the CHCT structure for Ge(111)- $\sqrt{3}$ Au. Structure saturates at 1.0ML, after which Au-Ge alloy droplets form on the completed $\sqrt{3}$ layer.

Annealing the sample has no effect on the ordering of Au on the surface until $\sim 600^{\circ}$ C, when Au goes through a phase transition to a (1x1) phase, which has not been previously observed. Further annealing of the sample produces no change, and the Au remains bound to the surface beyond the melting point of Ge. Thus, removing Au from the surface requires repeated cycles of ion bombardment and annealing.

As shown in the phase diagram (Fig. 1), the transition temperature between the $\sqrt{3}$ and (1x1) phases is weakly dependent on coverage. The transition temperature is $\sim 640^{\circ}\text{C}$ at 1.0ML of Au coverage but is reduced to $\sim 580^{\circ}\text{C}$ at 0.8ML and lower coverage. At the transition temperature, domains undergo fluctuations between the two phases. The transition happens at different temperatures for different sized domains on the surface. Smaller domains make the transition at slightly lower temperature than larger domains, as described in detail in Section 3.3.

3.2. Growth of Au on Ge(111) as Function of Coverage and Temperature

3.2.1 Coverage <1.0ML

Immediately after deposition of Au onto Ge(111) at 410°C, the LEEM image in Fig. 2(d) was measured. Then the sample was cooled to room temperature (~22°C) and transferred into the STM, where the three images in Fig. 2(a)-(c) were measured at different resolutions on the same region of the sample. Clearly the Au islands, such as the one marked by the white arrows in the three images, prefer to nucleate near step edges. Because of the high temperature growth, the Au presumably formed small islands of $\sqrt{3}$ structure, resulting in the observed 120° angle (white arrow) between two edges of this island, indicating crystalline order. Despite the clearly defined edges of the island, the atoms within the island are not resolved in Fig. 2(c), probably as a result of atomic motion. The growth of $\sqrt{3}$ regions is consistent with earlier STM observations that showed such regions forming on surfaces annealed to 300 or 500°C, ¹⁰ or deposited on Ge(111) held at 400°C or deposited at room temperature and annealed to similar temperature. ²⁸ The LEEM image of the same sample shows the Au islands as small dark features, which are distinct from the large black dots due to contaminated regions (Fig. 2(d)). By comparing the areas of the Au islands relative to the clean Ge, the sample coverage was calibrated as 0.16 monolayer (ML). While large contamination spots were typically seen near regions of high step density, they were not evident in the other images shown in this paper.

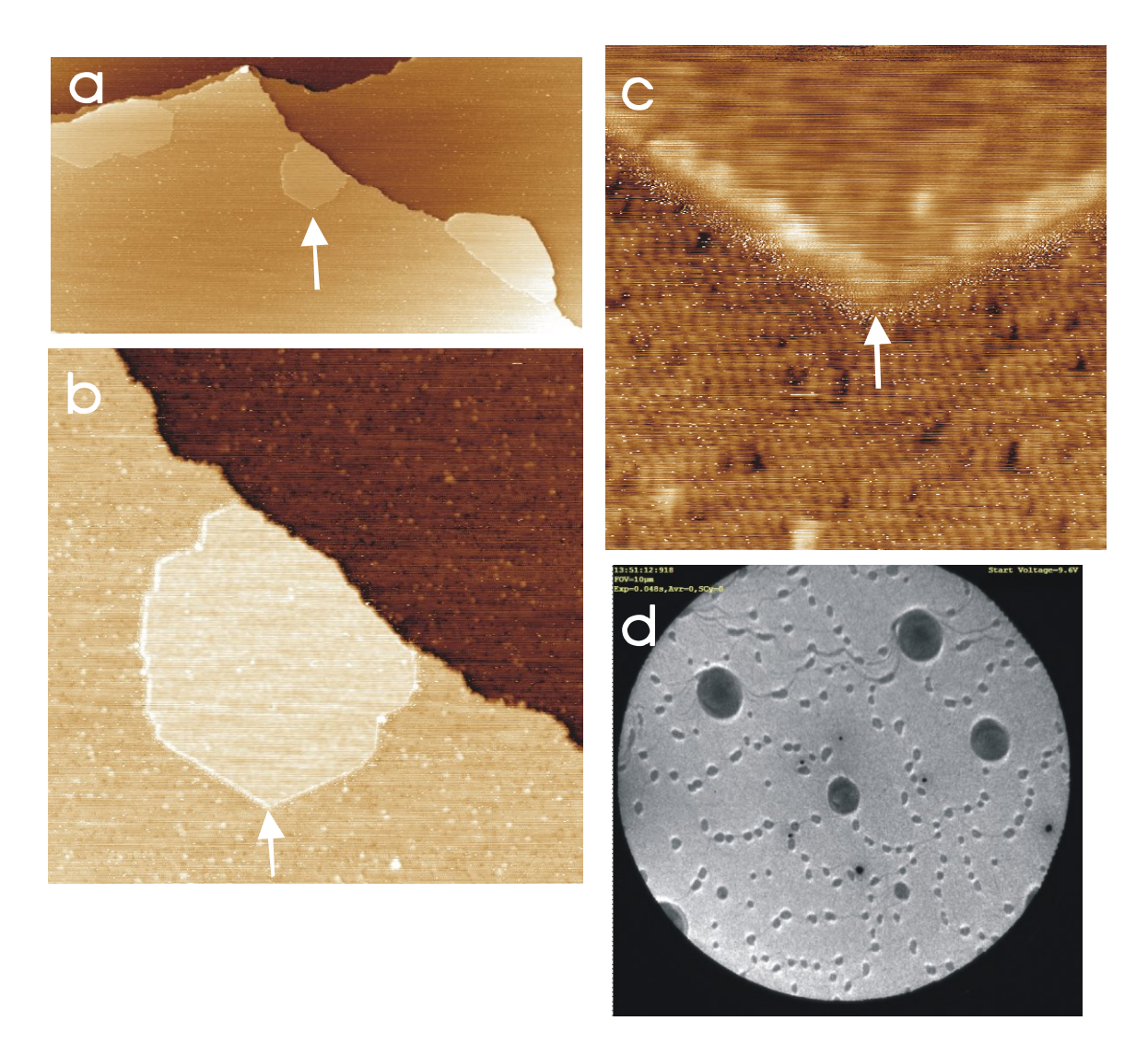


Fig. 2. (color online) STM and LEEM images of the same sample with 0.16 ML of Au deposited on Ge(111) at 410°C and cooled to room temperature for measurements. Au nucleates in small islands near step edges. Arrow marks same feature shown in three magnifications of STM images of the same area, (a) 7000Åx3500Å. (b) 1750Åx1740Å. (c) 250Åx250Å. High resolution features from the clean Ge(111) c(2x8) structure are observed in the bottom half of this image. For the STM images, V_{sample} +1V, I_{T} =0.5nA. (d) LEEM image, with electron energy 9.6eV, field of view (FOV) 10µm., shows small dark features ascribed to Au islands. Determination of the total area comprising Au islands relative to Ge regions gave the calibration of the Au coverage. Large black dots due to contaminated regions were subtracted from the areas used to determine the Au coverage.

When dosing above 1 ML Au at room temperature, LEEM images show no evidence of the island formation seen at higher temperatures, and LEED shows no evidence of the √3 phase or any other structure. This suggests that at temperatures below 200°C, the growth mode exhibits metastable Frank–van der Merwe (layer-by-layer) character. This behavior was seen by Venables

et al. in the similar system of Ag/Si(111)²⁹. Upon heating Au/Ge(111) above 200°C, islands become apparent in the LEEM images, and LEED shows the $\sqrt{3}$ structure. Thus, the system returns to its Stranski–Krastanov nature, with Au-Ge alloy droplets on top of a single $\sqrt{3}$ layer.

LEEM and LEED data from annealing or dosing Au onto Ge(111) above 200°C show the growth of the $\sqrt{3}$ layer, as reported by others studying this system. ^{10, 30-32} At such temperatures, thermal energy is sufficient to drive adatom diffusion on the surface, allowing the Ge(111)- $\sqrt{3}$ Au reconstruction to form. LEEM images obtained either by dosing at elevated temperature or by dosing at room temperature followed by annealing to higher temperatures, show similar surface structure, with no observable difference in the LEED or LEEM data for either growth parameter.

Fig. 3 shows a series of dark field LEEM images, taken with a $\sqrt{3}$ diffraction spot, at different coverages as Au was dosed onto Ge(111) at 400°C. At this temperature, LEED shows the expected $\sqrt{3}$ structure for Au coverages above 0.2 ML. The dark field imaging confirms that the bright areas of Fig. 3 have $\sqrt{3}$ order and that the dark areas are the Ge(111) surface. The growth of Au- $\sqrt{3}$ patches on the Ge(111) surface occurs by nucleation of small islands, which grow as more Au is deposited. This growth mode is well understood and has been described by Venables.³³ Up to the melting point of germanium, Au does not evaporate off the surface. Thus, it is safe to assume that growth proceeds in the regime of complete condensation. Surface dynamics are then reduced to the incoming flux of Au atoms, together with the interplay of adatom diffusion and capture by islands on the surface.

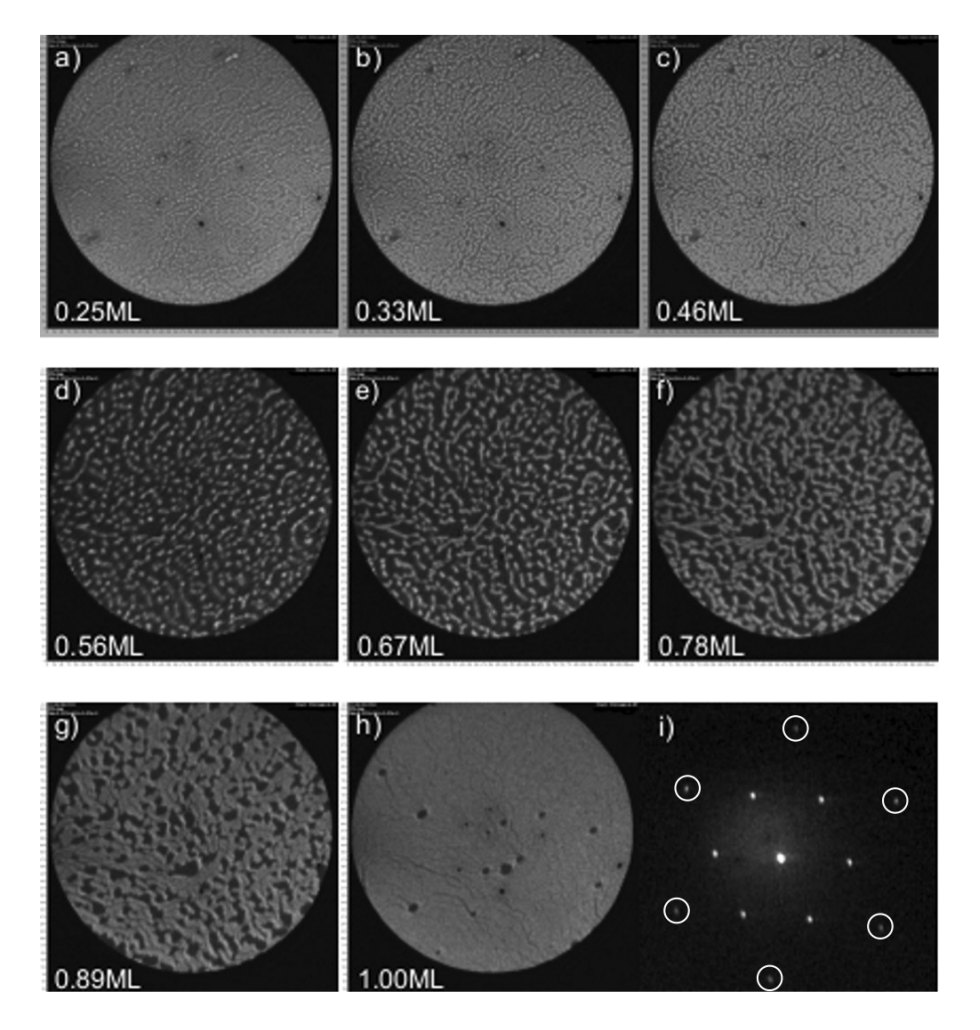


Fig. 3. Dark field LEEM images of growth of Au on the Ge(111) surface with increasing coverage, labeled on each image, as Au is dosed at 400°C. Bright areas have $\sqrt{3}$ order, and dark areas are the Ge(111) surface. (a–c) FOV 10 μ m; (d – h) FOV 5 μ m. Electron energy 6.0eV. (i) LEED pattern of the Au $\sqrt{3}$ phase (first order spots are circled in white).

3.2.1. Behavior of 3D Islands for Coverage >1.0ML

After completion of the first layer, additional Au islands begin to form on the surface. Fig. 4 shows a series of 3D islands growing on the surface as the Au coverage increases. Islands preferentially nucleate at kinks in the atomic steps of the Ge(111) surface. The 3D islands that form at temperatures above 250°C for coverage >1.0ML do not have any long-range order in their structure, as evidenced both by the lack of additional LEED spots and any contrast in the LEEM images at any electron energy. This is consistent with identification of the islands as

consisting of liquid Au-Ge alloy droplets, as previously seen for Au/Si(111).^{34, 35} This is also supported by the study of the Au-Ge catalyst used for vapor-liquid-solid (VLS) growth of Ge nanowires³⁶ and is consistent with the bulk phase diagram for Au-Ge (Fig. 5 of Ref. 37). These alloy droplets can begin to form at temperatures below the bulk eutectic temperature of 361°C, presumably because supersaturation of Ge in the growing alloy droplet can reduce the Au nucleation temperature.³⁷

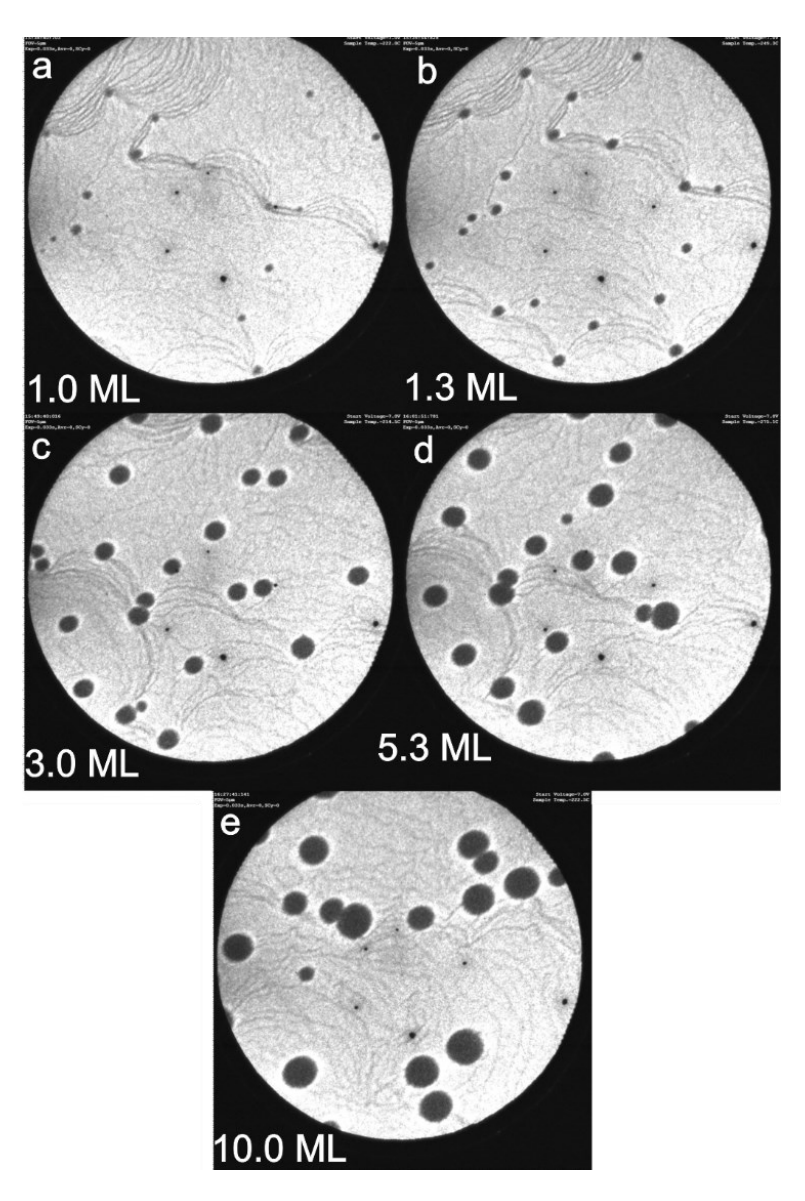


Fig. 4. Au deposition above 1 ML. All images are 5 μm FOV and were measured with 7.0 eV electrons. This sequence (a-e) shows the growth of 3D Au-Ge alloy droplets growing on top of the first complete Au layer.

Similar to other Stranski-Krastanov systems, the density of islands on the surface has a strong temperature dependence. This can be seen in Fig. 5, which shows the natural log of island density as a function of inverse kT, where k is Boltzmann's constant and T is absolute temperature. Taking an atomistic approach to the growth parameters of islands as 2-D clusters on a completed first layer, as described by Venables et al., 33 the cluster density is given as:

$$n_x \approx N_p(R)e^{\beta E}$$

where $N_p(R)$ is a number density factor which is dependent on a critical cluster size and a function of the dosing rate R, β is 1/kT, and E is the activation energy. The activation energy is found from Fig. 5 to be 1.07 eV, which is in good agreement with a recent paper on Au/Ge(111).³⁸

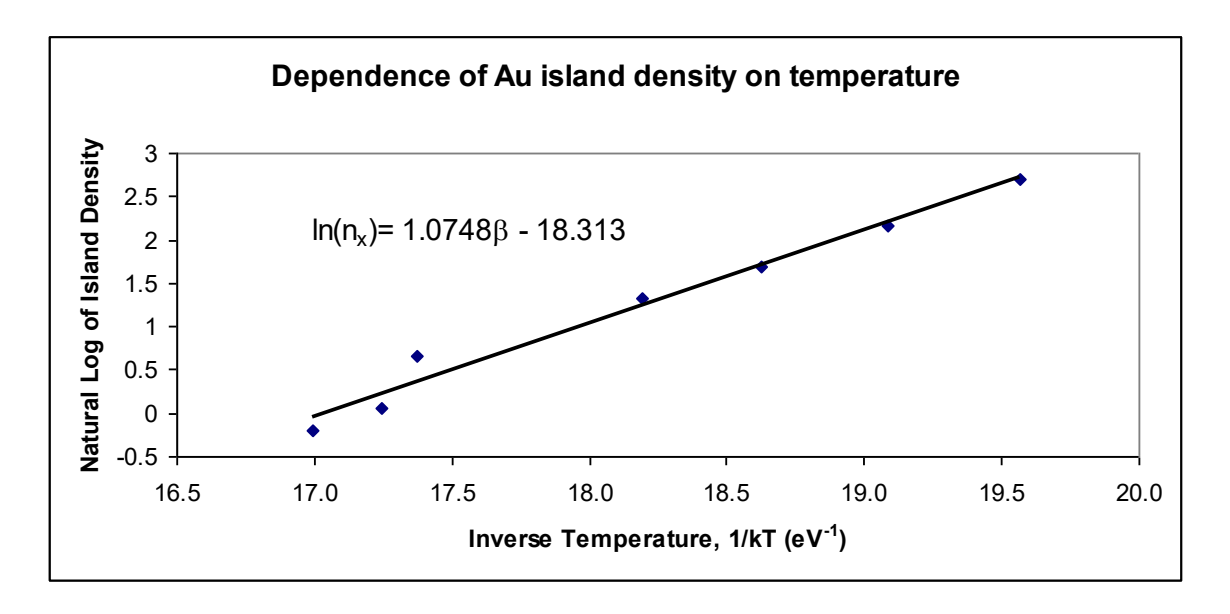


Fig. 5. Plot of the natural logarithm of the Au island density versus the inverse of kT ($\beta = 1/kT$). This shows the exponential relationship between the number of islands which grow on the first layer of Au and the temperature at which the Au is deposited.

While the previous discussion focused on experiments involving the dosage of Au onto a hot surface, the growth of Au dosed at low temperature and then annealed is very similar. Fig. 6 shows a series of images taken as a sample with 6.0 ML of Au was heated from 200°C to 410°C.

Below 250°C, there was no particular ordering of the Au on the surface as evidenced by the lack of any LEED pattern. Heating the sample above 250°C allows the formation of the √3 structure of the first Au layer, and the Au-Ge droplets grow on top of that layer. At lower temperatures, many small droplets first begin to coalesce on the surface. As the temperature is raised, these droplets undergo Ostwald ripening, and smaller islands begin to shrink as larger islands begin to grow. The final image in the series shows only a few large islands on the surface, compared with the many smaller ones that existed at lower temperatures.

Fig. 7 shows the effect of dosing 10 ML Au onto the surface at 400°C, with the formation of 3D islands, followed by cooling the sample to 50°C. As the surface is cooled below 200°C, the islands begin to shrink to about 50% of their higher temperature size. As the islands shrink, their boundaries take on a harder, more angular edge, with some of the islands developing a hexagonal shape, as they begin to crystallize on the surface. Nevertheless, no LEED pattern was observed, suggesting that there is no long-range order. The white spot that appears near the center of the islands when they are cooled may be another sign of the change in crystallinity. If the sample is heated again, the islands will again become rounder and larger, so that they look as they did when they were dosed.

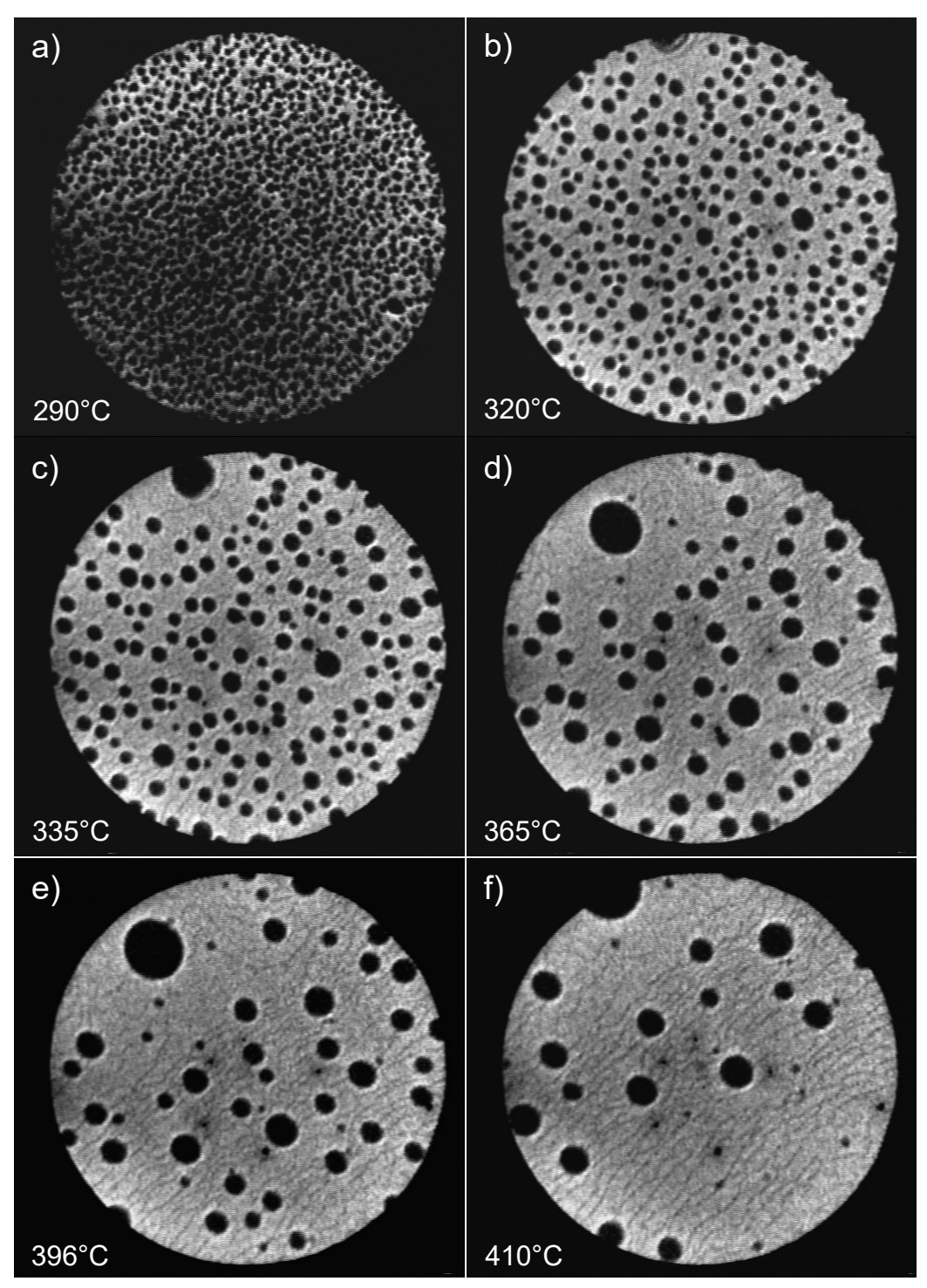


Fig. 6. (a-f) Series of LEEM images of Au/Ge(111) taken as the temperature was rising after dosing 6.0 ML of Au at 200°C. The surface initially has many small Au-Ge alloy droplets at low temperature, with Ostwald ripening occurring as the temperature is raised, producing fewer but larger islands. FOV 5 μ m, electron energy 6.5 eV.

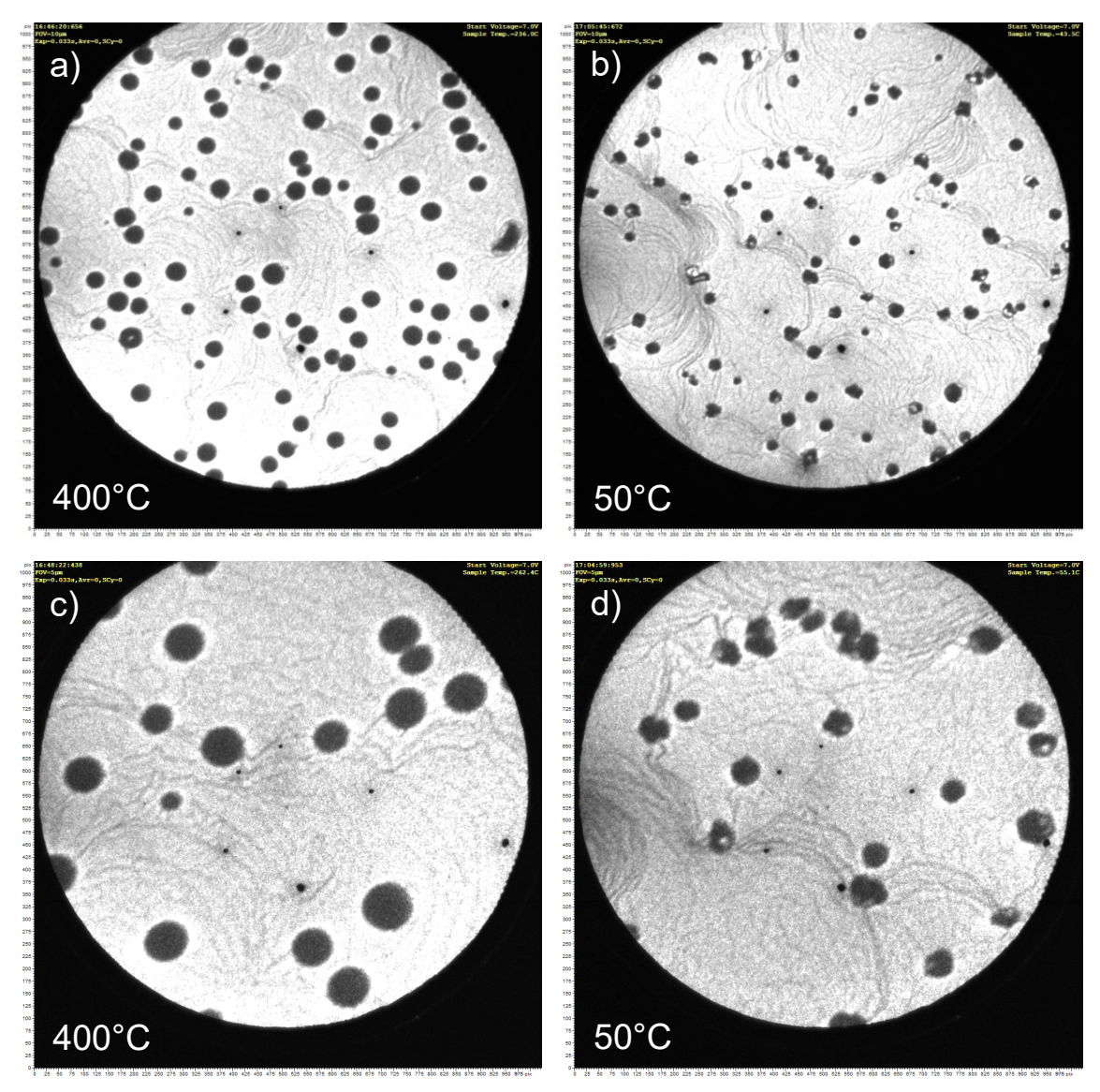


Fig. 7. Au was dosed to 10 ML on the sample at a temperature of 400°C, and then the sample was cooled to near room temperature. (a-b) FOV 10 μ m. (c-d) FOV 5 μ m. As the temperature is lowered, the islands shrink, and their round edges become sharper and more angular, with some looking hexagonal in shape.

3.3. First Order Reversible $(\sqrt{3}x\sqrt{3})R30^{\circ}$ to (1x1) Phase Transition of Au/Ge(111)

One of the unique traits of LEEM is its ability to image surfaces in real time while dosing or heating the sample, allowing the observation of dynamics of surface processes, such as the transition between different surface structures. As a real-space imaging method with information on the diffraction pattern of domains, LEEM is well suited to studying surface structural phase transitions. By imaging the surface with greater resolution than the size of the phase domains, the

coexistence of two distinct phases with an abrupt boundary indicates that the transition is first order; otherwise, it is second order. LEEM has been previously used with considerable success to characterize surface phase transitions, 39,40 such as the determination by Telieps and Bauer that the reversible Si(111)-(7x7) to (1x1) phase transition was first order. 41,42

For the Au/Ge(111) surface, there are only two phase transitions: the low temperature disorder to $\sqrt{3}$ transition and the high temperature $\sqrt{3}$ to (1x1) transition. Below about 200°C, Au mobility on the surface is severely restricted, and the formation of structures with long-range order is not energetically possible. Above 200°C, we find the rapid onset of the $\sqrt{3}$ phase across the entire surface as the adatoms order themselves to reduce the surface free energy. As the temperature continues to rise, the $\sqrt{3}$ phase persists without change up to about 600°C, where the surface transitions to a (1x1) phase to further reduce the surface free energy. The (1x1) phase persists at higher temperatures until the Ge sample melts.

3.3.1. Temperature and Coverage Dependence of the $(\sqrt{3}x\sqrt{3})R30^{\circ} \leftrightarrow (1x1)$ Transition

Fig. 8 shows a series of LEEM images as the $\sqrt{3}$ phase (bright areas) evolves into the (1x1) phase (dark areas) as the temperature is first increased by a few degrees, and then the reverse transition when it was decreased by a similar amount. These images were taken with an initial Au coverage of more than 1.0 ML at a temperature of 640°C. At this temperature, most of the Au-Ge alloy droplets present on the surface above 1.0 ML of coverage have desorbed. The two black circles on the top of the first image are Au-Ge alloy droplets that are still present after most have desorbed from the surface. In the second image the top right island has desorbed; after that, the left island also desorbs. The dark round feature at the bottom of the image, however, is a surface defect. The LEEM images show a definite separation of the two phases, with boundaries occurring between the $\sqrt{3}$ and (1x1) phases in coexistence, showing that this is a first order

transition, similar to the (4x4) to (1x1) transition of Ag/Ge(111) system⁴³, but unlike the second order transition from $\sqrt{3}$ to (1x1) observed for Au/Si(111).³⁴

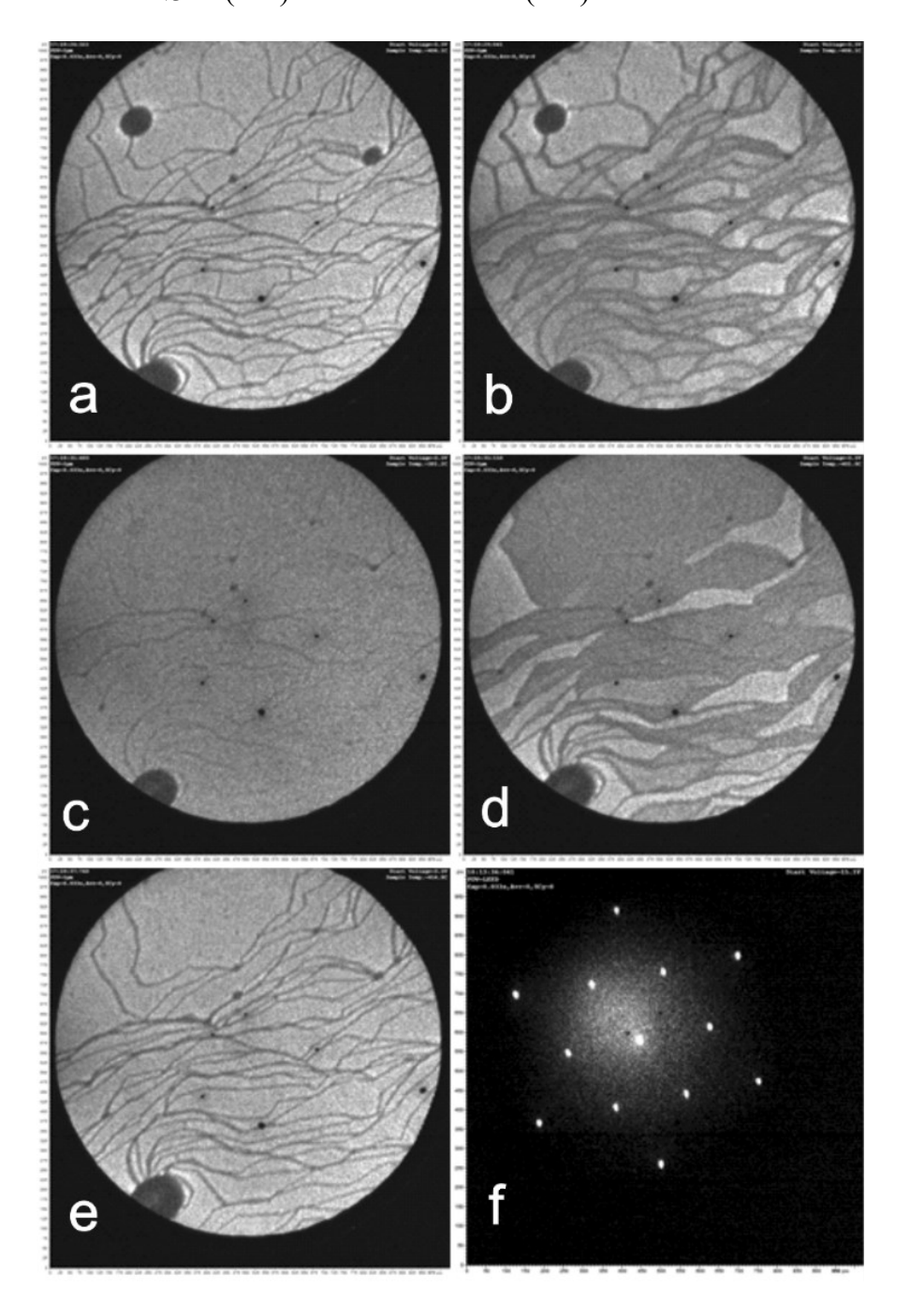


Fig. 8. In this series of LEEM images(a-e), we begin with >1 ML of Au at 640°C. At this temperature most of the Au-Ge alloy droplets have desorbed, but two can still be seen at the top of the first image. The $\sqrt{3}$ phase has bright contrast, and the (1x1) phase has dark contrast in these images. The (1x1) phase begins to grow from the steps and domain boundaries as the phase transition proceeds. After completely transforming to the (1x1) phase in (c), the temperature was lowered several degrees and the transition reverses. Eleven seconds have elapsed from the first image to the last image. FOV 5 μ m. (f) LEED pattern of the $\sqrt{3}$ phase.

Fig. 8 shows that the phase transition originates at steps and domain boundaries. There is no evidence in any of the LEEM data to suggest that the phase transition can nucleate in the middle of a terrace without an activation center such as a step or phase boundary. In the image sequence most of the steps are running in a more-or-less horizontal direction. The divisions that run in a more vertical direction are domain boundaries that separate different nucleation domains when the Au is first dosed onto the sample. In the first two images, these domain boundaries act similarly to the steps in that the phase transition begins here and then moves inward on the terraces. As the temperature is lowered and the $\sqrt{3}$ phase grows back, these domain boundaries are gone. This can be seen by comparing Fig 8(a) with Fig. 8(e), especially in the upper left area where the terraces are larger. There are a number of step-like features in the first image that do not exist in the last image. These are the adsorption domain boundaries that are absent when the $\sqrt{3}$ phase regrows as the sample is cooled from the transition temperature.

When the sample is cooled, the nucleation of the $\sqrt{3}$ phase begins on the terrace and then propagates outward towards the steps that bound it, as shown in Fig. 9, which shows a sequence of consecutive frames of a different sample during a similar experiment. Fig. 8 shows that larger terraces take longer to transform from $\sqrt{3}$ to (1x1) during heating, whereas Fig. 9 shows that larger terraces transition first from (1x1) to $\sqrt{3}$ when cooling.

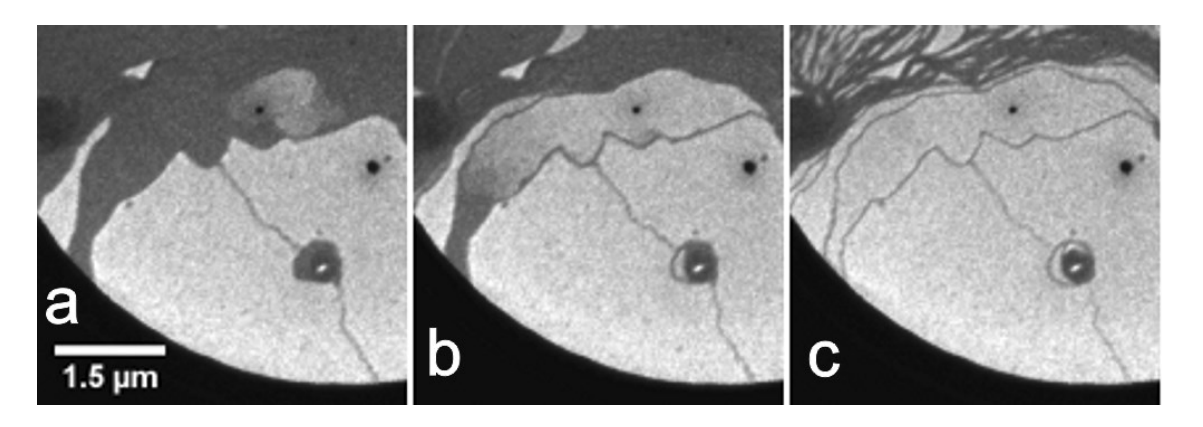


Fig. 9. (a-c) A sequence of consecutive frames from a LEEM video at 1 frame per second. The sample has been cooled below the transition temperature, and the (1x1) phase (dark areas) is transitioning to the $\sqrt{3}$ phase (light areas). Notice that the transition begins on the terraces and then continues outward toward the steps.

Looking at Figs. 8 and 9, it is clear that the entire surface does not undergo the phase transition at the same time. Indeed, it can be seen in the images that some of the domains undergo the phase transition before others. This is true in both directions, $\sqrt{3} \rightarrow (1x1)$ and $(1x1) \rightarrow \sqrt{3}$, as seen in Fig. 8. This non-homogeneity in the phase transition is due to a spread in the transition temperature, $\sim 2^{\circ}$ C, over which the transition begins and completes. A temperature gradient across the sample surface was ruled out as the cause for the temperature width of the coexistence region based on the observation of phase fluctuations between the two phases, which is discussed in more detail below.

This effect of a first order phase transition having a soft transition temperature instead of an abrupt transition at a critical temperature has been observed for other surface phase transitions, such as the Au/Si(111) (5x1) to (1x1) transition studied by Swiech et al.³⁴ and the Si(111) (7x7) to (1x1) transition as reported by Hannon and Tromp.³⁹ For both of these phase transitions, the coexistence range was on the order of 10°C, and surface strain was suggested as the most likely reason for the transition temperature range. Essentially, the strain fields on the surface, most notably from step structures, impose a force on the phase domains, making it

energetically favorable to form boundaries between the phases that produce repulsion between regions of the same phase. This causes a metastable state where phase coexistence is preferred near the transition temperature. In Figs. 8 and 9, this effect is evident in the Au/Ge(111) $\sqrt{3}$ to (1x1) phase transition, where the temperature was ramped quickly through the transition temperature. Around the steps is a region where the phase transition occurs first in going from $\sqrt{3}$ to (1x1) or occurs last in going from (1x1) to $\sqrt{3}$. This indicates there is repulsion between the $\sqrt{3}$ domains, which would be consistent with step induced strain fields causing the phase coexistence.

The phase diagram shown in Fig. 1 shows a hatched coexistence region between the $\sqrt{3}$ and (1x1) phases, which is exaggerated in the figure to make it easily noticeable. At higher coverages, the phase transition occurs at slightly higher temperatures. The average transition temperature is about 640°C for 1ML of Au coverage. Lowering the coverage reduced the transition temperature to 600°C at 0.75 ML and to 580°C for both 0.60 and 0.50 ML coverages.

Although the Au/Ge(111)–(1x1) phase has a similar LEED pattern to that of the Ge(111) substrate, the LEEM images at submonolayer coverage show a separate contrast that is different from those of either the Au- $\sqrt{3}$ or the underlying Ge surface, as shown in Fig. 10. This suggests that these two (1x1) phases have different structure, even though they have the same periodicity. Note that this is different from the Ag/Ge(111)–(1x1) phase, which has no distinguishable LEED pattern or LEEM contrast from that of the underlying Ge(111).

Fig. 10 shows a 0.60 ML Au covered surface as it transitions from the $\sqrt{3}$ to the (1x1) phase. The sample was held at a constant 580°C, and about 1.5 minutes elapsed between Fig. 10(a) and (f). In Figs. 10(b-d), three different contrasts occur: bright- $\sqrt{3}$, dark-Ge(111), and dark grey-(1x1). There was no difference in the LEED pattern for the dark-Ge(111) and dark grey Au-

(1x1). Although there must be some structural difference that gives rise to the different contrast in LEEM, these experiments did not determine what that difference is. The Au-(1x1) phase was determined because the dark areas persist below the transition temperature and are therefore the Ge substrate, and the dark grey contrast only appears when the transition temperature is reached. This is a reversible phase transition and cooling the sample from Fig. 10(f) returns the $\sqrt{3}$ phase.

We estimate the coverage of the Au-(1x1) phase by carefully examining the $\sqrt{3}$ to (1x1) phase transition, measuring the areas corresponding to these two phases, and using the known coverage of 1.0 ML for the $\sqrt{3}$ phase. Assuming conservation of Au atoms during the phase transition, the number of Au atoms in the transformed $\sqrt{3}$ areas must be equal to the number of atoms in the new (1x1) areas, $\Delta A_{\sqrt{3}} \cdot \theta_{\sqrt{3}} = A_{(1x1)} \cdot \theta_{(1x1)}$, where $\Delta A_{\sqrt{3}}$ is the change in area of the $\sqrt{3}$ phase, $A_{(1x1)}$ is the area of the (1x1) phase, and θ is the coverage of the respective phase. Using the ImageJ program⁴⁴, we measured the area of the $\sqrt{3}$ regions in Fig. 10(a). Then we measured the $\sqrt{3}$ areas and the (1x1) areas in images 10(b-d). Subtracting the $\sqrt{3}$ area in these three images from that in Fig. 10(a) indicates how much of the $\sqrt{3}$ phase transformed, $\Delta A_{\sqrt{3}}$, in each of these three images, 10(b-d). Substituting into the given equation, we determine that the average coverage of the (1x1) phase is 0.367 ± 0.002 ML. Note, however, that this discussion does not prove that the coverage of the (1x1) structure is always fixed at this number.

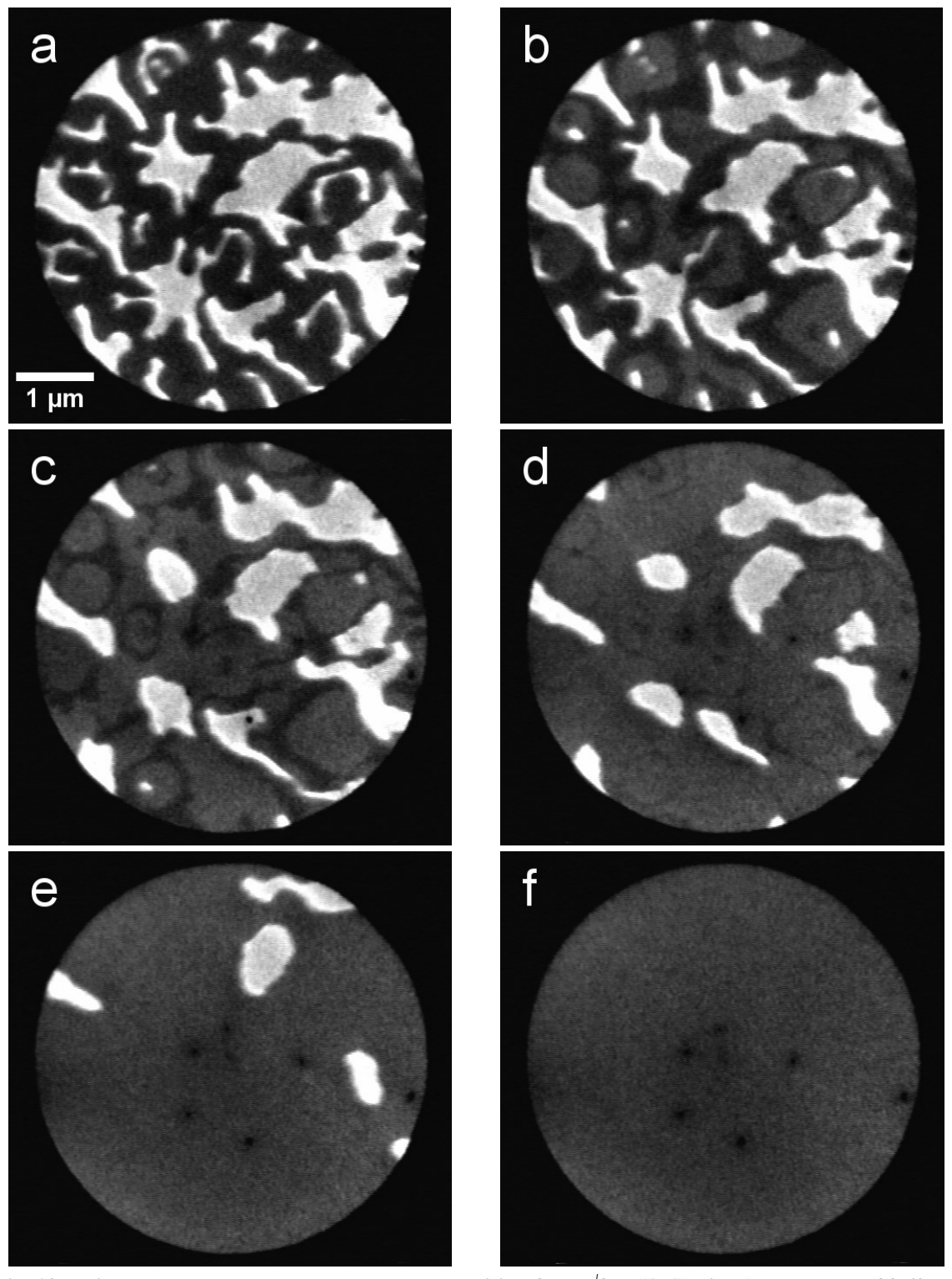


Fig. 10. This LEEM sequence shows the phase transition from $\sqrt{3}$ to (1x1) with Au coverage of 0.60 ML. Sample temperature is 580°C. $\sqrt{3}$ is bright, Ge substrate is dark, and (1x1) is a dark grey. a) shows the $\sqrt{3}$ phase on the Ge substrate. b) shows the $\sqrt{3}$ beginning to transition to the (1x1). Notice that the (1x1) phase is distinguishable from the substrate contrast. c)-d) the transition nears completion. e) the (1x1) phase now covers the entire surface except where $\sqrt{3}$ domains still exist. f) The transition is complete.

3.3.2. Fluctuations in the $(\sqrt{3}x\sqrt{3})R30^{\circ} \leftrightarrow (1x1)$ Phase Transition

The contrast between the $\sqrt{3}$ and (1x1) phases in the LEEM images was originally distinguished using dark field imaging. While exploring the coexistence region between these two phases, an unexpected behavior was found. For samples with 1 ML of Au that are within the coexistence region, small domains switch back and forth between the two phases. If the sample is taken rapidly through the transition temperature, as in Figs. 8-9, we find the more typical first order transition described in Sect. 3.3.1. However, if the sample temperature passes slowly through or is held in the coexistence region, even for a few seconds, small domains will fluctuate between the two phases. LEEM is the perfect tool to view and characterize a dynamic event like this because of its real-space, real-time data acquisition with the ability to capture data at video rates. Fig. 11 shows a series of images of a 1.0 ML Au covered Ge(111) surface at a constant temperature of 635°C, taken from the movie available in Supplementary data S1. The images show the $\sqrt{3}$ and (1x1) phases coexisting on the sample as bright and dark areas respectively. The domains circled in red in the images show how the phase switches back and forth between the two structures.

To further elucidate the phase switching phenomenon, a Canny edge detector⁴⁵ was used to process a sequence of 300 video frames (10 seconds of video) beginning with the first image in Fig. 11. The Canny edge detector was implemented in ImageJ⁴⁴ using the FeatureJ⁴⁶ plugin. The edge processed images were then averaged together to produce the image in Fig. 12(a). Edges with the darkest contrast were present during the entire video sequence, whereas the lighter edges show areas where domains were fluctuating. Indeed, some of these are the same as the domains indicated in Fig. 11. Using this technique, the fluctuating domains were identified and their sizes recorded. The average size of a fluctuating domain was found to be 12000 nm².

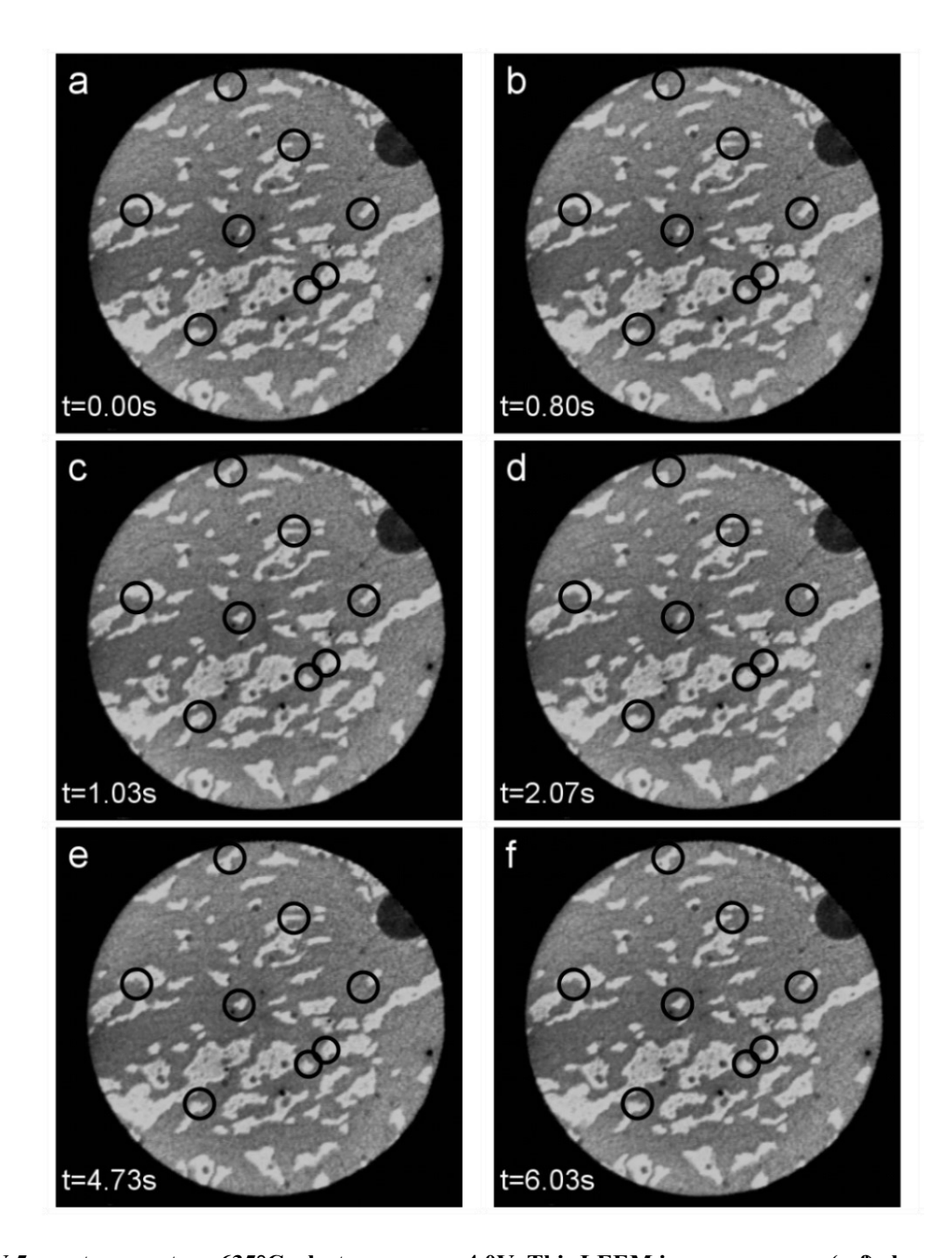


Fig. 11. FOV 5 μ m, temperature 635°C, electron energy 4.0V. This LEEM image sequence (a-f) shows a 1.0 ML Au covered Ge(111) surface in the coexistence region of the $\sqrt{3}$ to (1x1) phase transition. Some of the domains are seen to fluctuate between the two phases. The black circles guide the viewer to some of the domains that are fluctuating in this sequence. The times relative to the first video frame are inset in each image.

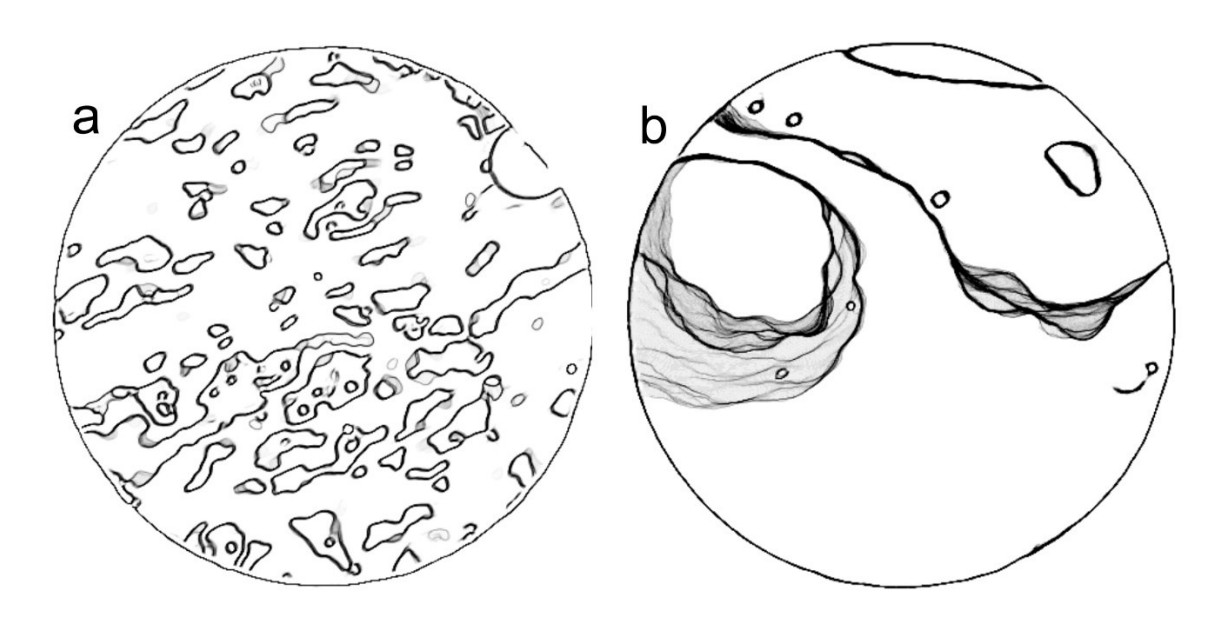


Fig. 12. (a) This is a time averaged image from 300 consecutive video frames of the LEEM image sequence in Fig. 11, after Canny edge detection was applied to each frame. The weight of the edges is proportional to the number of frames for which that edge appears in that position. The lighter grey edges seen in the image are domains that were undergoing fluctuations. (b) Same type of time averaged image with Canny edge detection for LEEM image sequence in Fig. 14.

The fluctuating domains do not alter in size during their lifetimes or due to differing temperatures. The temperature range of the coexistence region is small but fluctuations that occur near the completion of the (1x1) phase have the same average size as fluctuations that occur near the completion of the $\sqrt{3}$ phase or anywhere between the two phases. Also, it is clear from the LEEM images that this is still a first order transition, as the phases are clearly separated. These phase fluctuations can even occur over hour long periods of time, where small changes in the temperature spanning the 2°C range over which the fluctuations occurred could be used to adjust the proportion of $\sqrt{3}$ to (1x1) coverage. The intermediate state between the complete phases existed within this temperature range and was consistent over multiple experiments. This behavior rules out a temperature gradient as the origin of the 2°C range for the transition temperature.

Figure 13 shows the intensity change within the marked squares as a function of time, from the same LEEM sequence as Fig. 11. The change in intensity between Fig. 13(a) and (b) is

due to one domain fluctuating between (1x1) and the $\sqrt{3}$ phases, as seen in the insets, which show a magnified view of the domain used in the intensity measurement. Therefore, the measured time dependence indicates the time for this domain to transition between the two phases., and Figure 13 (c) shows that the domain fluctuates between two well defined states, as expected in a first order transition. Although the length of time that the domain stays in any one state appears to be random, the switching time is consistent and was found to be 130 ± 30 milliseconds, as shown in Figure 13(d).

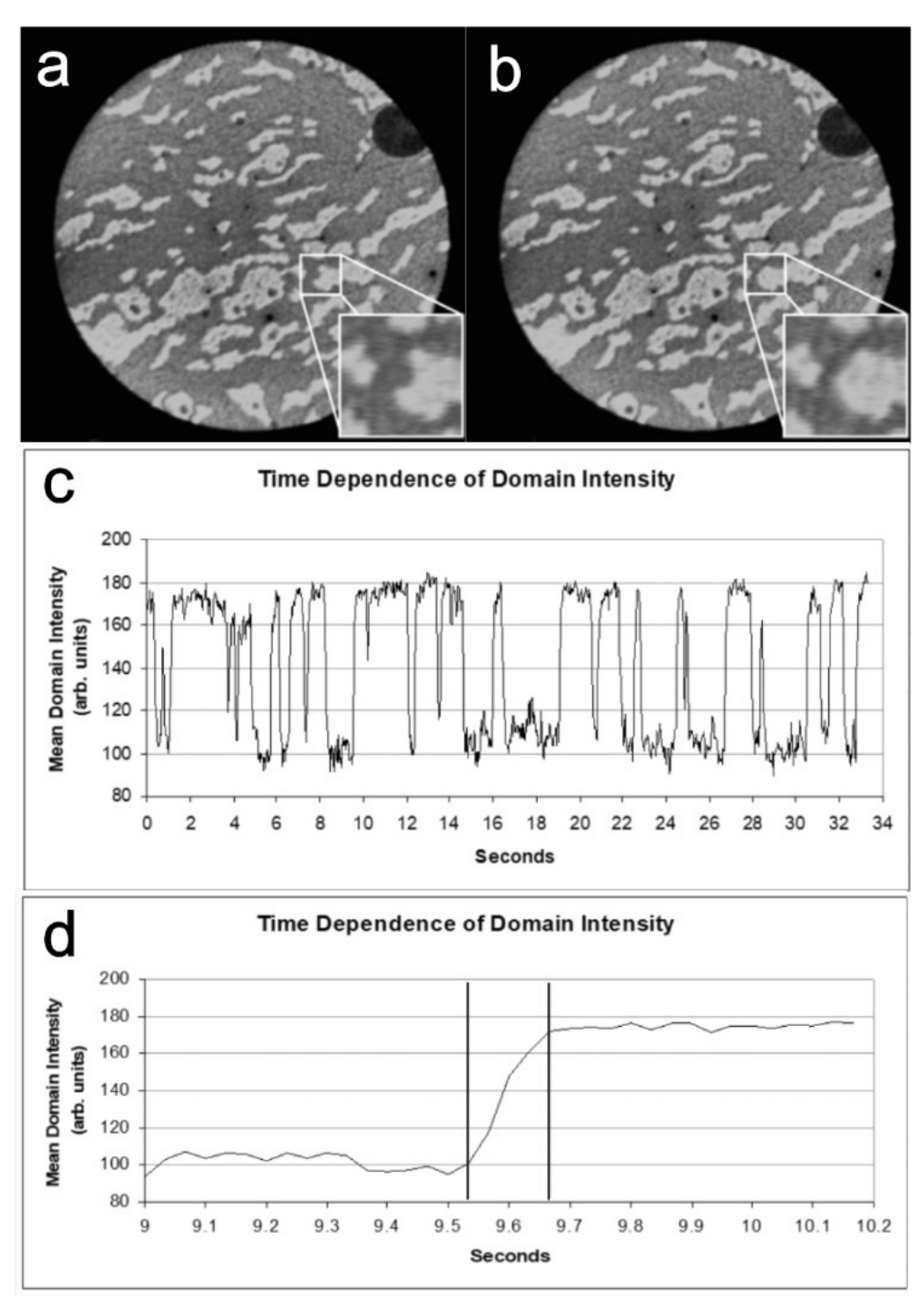


Figure 13. FOV 5 μ m. From the sequence of LEEM images in Fig. 11, the time dependence at 635°C of the fluctuating domain within the indicated squares. a) and b) show the (1x1) (dark) and $\sqrt{3}$ (bright) phases of the domain respectively. c) Plot of the time dependence of the domain switching between two distinct phases. d) Scaled view of the transition from the (1x1) phase to the $\sqrt{3}$ phase, showing that it takes ~130mS to complete the transition.

We now compare the behavior of the $\sqrt{3}$ domains for a low step density sample, which has large terraces. The corresponding Au domains are also large, mostly being only bound by the step edges themselves. In the coexistence region, the phase boundary between the $\sqrt{3}$ and (1x1) phases is kept to a minimum by producing fewer and larger domains. The fluctuations present on this surface are now boundary fluctuations instead of domain fluctuations. The phase boundary itself fluctuates in size, shrinking back to produce a larger (1x1) domain or growing out to produce a larger $\sqrt{3}$ domain. Fig. 14 shows a short sequence of images where the boundary is fluctuating, taken from the movie available in Supplementary data S2. In the video, the boundaries are in constant motion and appear fluid, as though there were a pushing match between the two phases; sometimes one gains more ground, and sometimes the other gains more ground. These large domains are much less stable than the smaller ones in Fig. 11, where the small domains fluctuating between the two phases do not change size and have fixed domain boundaries. On the other hand, for the larger domains in Fig. 14, the boundary fluctuates so that the domains are always changing size. Since these boundary fluctuations are not fixed or constrained as are the small domains, the overall sizes of the domains shrink and grow by amounts many times the area of the fluctuations. In Fig. 14(a), the large domain on the left is at its maximum size in the sequence; in Fig. 14(c), it shrinks to its minimum size; and then in Fig. 14(d), it has grown again. Note that these boundary fluctuations are still present even if the temperature is held constant somewhere within the coexistence region.

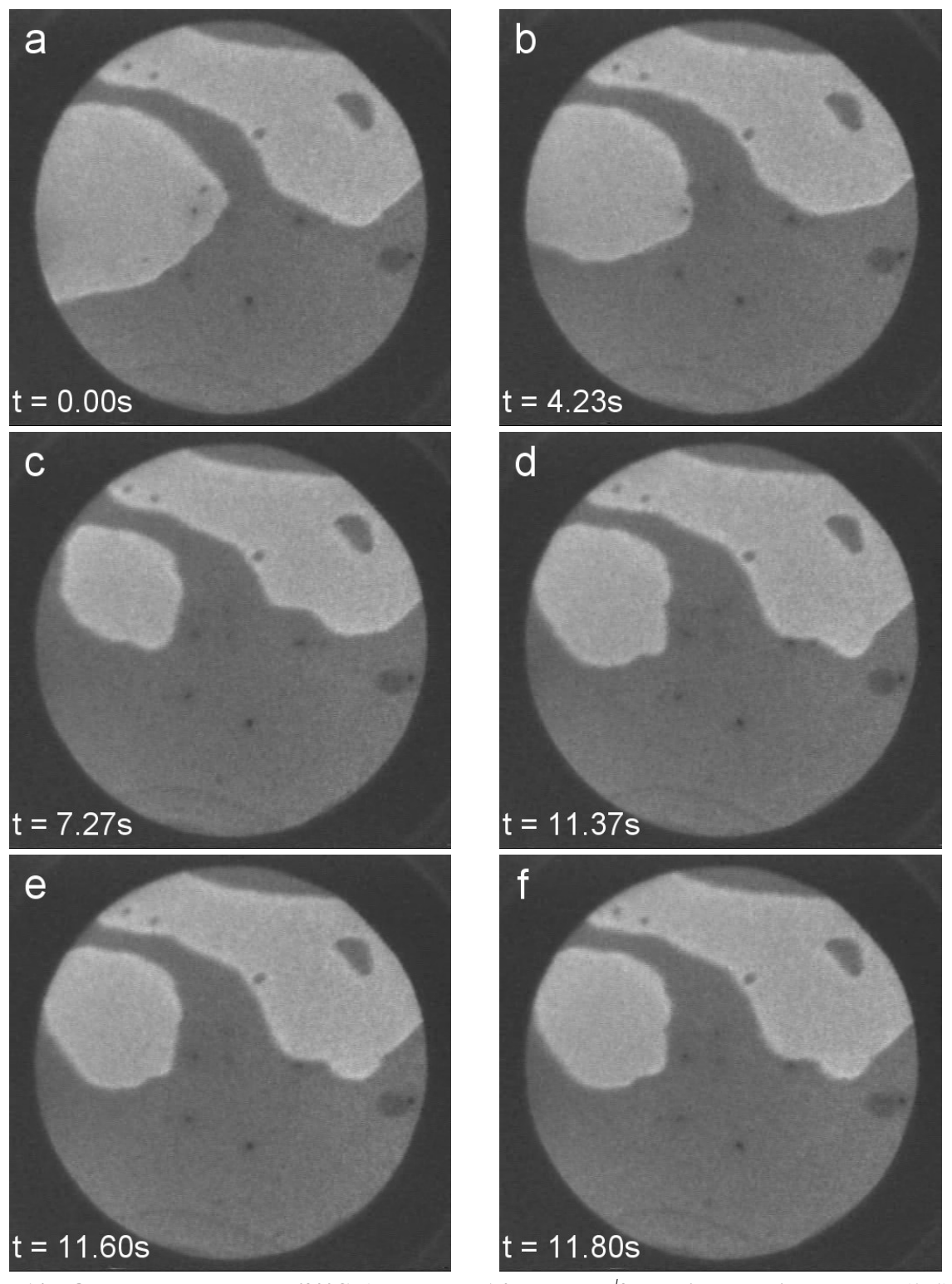


Fig. 14. FOV 5 μ m, temperature 630°C, Au coverage 1.0 ML. The $\sqrt{3}$ domains are bright, and the (1x1) regions are dark. This sequence of LEEM images (a-f) from the coexistence region shows how the domain boundaries of large domains change in the same temperature range where smaller domains fluctuate. Note particularly how the phase boundaries change from image to image. The times relative to the first video frame are inset in each image.

To better convey the movement of the domain boundaries in Fig. 14, a Canny edge detector, as described above, was used to find all the edges of a sequence of video frames, and the edge frames were averaged to produce the image in Fig. 12(b). As before, the averaging creates an image of the edges where the darkness of the edge is a function of its motion throughout the sequence. The more a boundary moves, the lighter it appears in the average. Fig. 12(b) shows that not all boundaries move or fluctuate. Also, the boundary fluctuations are not as discrete as were the domain fluctuations in Fig. 11 and 12(a), and the boundaries have more freedom to fluctuate to different geometries. Boundaries that fluctuate are presumably not pinned.

3.3.3. Possible Mechanism for Phase Fluctuations of the $\sqrt{3}\leftrightarrow(1x1)$ Au/Ge(111) Transition

Similar phase fluctuations have been reported previously for the $\sqrt{3}$ (β phase) to (1x1) transition of Pb/Ge(111) using LEEM by Sato et al. ⁴⁷⁻⁴⁹ They found that the difference in the number of atoms between the β and (1x1) phases of an average domain size (8500 nm²) is of the same order, hundreds of atoms, as the thermal fluctuation in the number of atoms derived from statistical mechanics. Therefore, the phase fluctuations are thermally driven because of the small area of the domains and the closeness in the coverage of the β and (1x1) phases in the coexistence region (1.303 and 1.29 ML, respectively).

At first glance, it would seem that the Au/Ge(111) system is very similar and that the fluctuations could be driven by the same mechanism. However, the coverage difference between the $\sqrt{3}$ and (1x1) phases for Au/Ge(111) is very large, 1.0 ML and 0.367ML, respectively. This produces a large difference in the number of atoms between the two phases for a typical domain of 12000 nm². Performing the same analysis as Sato et al., the thermal fluctuations in the number of atoms is on the order of hundreds of atoms but the difference in the number of atoms between

the two phases based on the coverages is tens of thousands of atoms. Thus, thermal fluctuations cannot drive the phase fluctuations when there is such a large difference in the coverage of the phases.

This leads us to speculate that a surface soft phonon can be responsible for the $\sqrt{3}\leftrightarrow(1x1)$ surface phase transition on Au/Ge(111), together with the associated phase fluctuations. Soft phonon modes are recognized as explanations for structural phase transitions in 3D bulk materials⁵⁰, such as SrTiO₃ and the well-known ferroelectric, BaTiO₃. They have more recently been invoked to explain several surface phase transitions, such as the surface charge density wave (CDW) associated with the Pb/Ge(111) $\sqrt{3}$ to (3x3) transition near -20°C, ^{51,52} the $\sqrt{3}\leftrightarrow(3x3)$ phase transition of Sn/Ge(111), ^{53,54} and the reversible (4x1) quasi-1D phase of In/Si(111) transitioning to an (8x2) phase with an accompanying metal-insulator transition. ⁵⁵ Thus, it is plausible that soft phonons could also be associated with the $\sqrt{3}\leftrightarrow(1x1)$ surface phase transition on Au/Ge(111), but this would need to be confirmed with theoretical molecular dynamics calculations, such as those done previously for Ag/Ni(100) and Ag/Cu(100). ⁵⁶⁻⁵⁸ We note, however, that there is no evidence for a CDW transition on Au/Ge(111) between the temperatures of 10K and room temperature. ⁵⁹

The phase coexistence observed for the $\sqrt{3} \leftrightarrow (1x1)$ transition on Au/Ge(111) is familiar from other surface phase transitions, such as the transition of Si(111) from the ordered (7x7) structure to a disordered (1x1) phase near $T_c \approx 860^{\circ}\text{C}$, which was studied by Hannon et al. using LEEM.⁶⁰ They determined that long-range elastic and electrostatic interactions are responsible for the surface phase coexistence in the Si(111) phase transition over a broad temperature range near T_c . After examining the entropy of the phases and the latent heat of the transition, they predict that phase coexistence is a universal feature of surface phase transitions. When heated from below T_c , the (1x1) regions grow and broaden between the (7x7) regions, which they

describe as domain wall premelting. Feenstra et al.⁶¹ used STM to observe similar 2D premelting behavior for the Ge(111) c(2x8) to (2x1) phase transition near 300°C. They saw the disordered regions forming at domain boundaries and then growing continuously with temperature until the entire surface becomes disordered.

3.4. Motion of Au-Ge alloy droplets on Ge(111) For Coverages Above 1 ML

Au-Ge alloy droplets on the $\sqrt{3}$ -Au covered surface become mobile at $\sim 300^{\circ}$ C. These are large 3D islands containing at least tens of thousands of atoms that move as a single cohesive unit across the surface at surprising speed. Fig. 15, from the movie available in Supplementary data S3, shows LEEM images with FOV 5 μ m, measured during Au deposition, in which multiple Au-Ge alloy droplets move on the surface. Many islands move in a jumping motion from one spot to another, and they tend to hop from position to position with no continuous motion at any temperature. Some 400 nm diameter islands can jump up to 1000 nm in 1 second. Although the island size is related to the temperature, no temperature dependence on the number of islands that move or the measured hopping distances could be discerned. Looking closely at the motion of the islands, they appear to initially be stuck in place and suddenly break free, sliding along the surface until they get stuck again. As the islands move, they change the step structure of the Ge, leaving a kink in the step that points in the direction of travel of the island (see additional red lines drawn in Fig. 15(a)). The island motion was always perpendicular to the steps.

Similar motion of 3D Au islands at ~327°C was first observed by Swiech et al. in a LEEM study of Au/Si(111).³⁴ The mechanism for the motion was elucidated by Curiotto et al. in their later LEEM study of Au/Si(111),³⁵ for which very similar island motion was observed as in our LEEM movies for Au/Ge(111). By comparing with the bulk phase diagram for the Au-Si

system, they determined that the 3D islands are composed of Au-Si alloy droplets which move perpendicular to the steps when more Au is added or when the temperature increases. When the droplet approaches a Si step edge, Si dissolves into the droplet and then comes to a chemical equilibrium according to the bulk phase diagram, resulting in the motion of the droplet up the step with stick-slip behavior, accompanied by changes in the Si step structure behind the advancing droplet. More recently, the same group has reported additional details about the behavior of Au-Ge alloy droplets on Ge(111).^{38, 62, 63} Similar behavior of the movement of liquid eutectic islands induced by sample temperature gradients was observed previously for Pt/Si(001)⁶⁴, Pt/Ge(110)⁶⁵, Au/Si(110)⁶⁶, and Au/Ge(110).⁶⁷

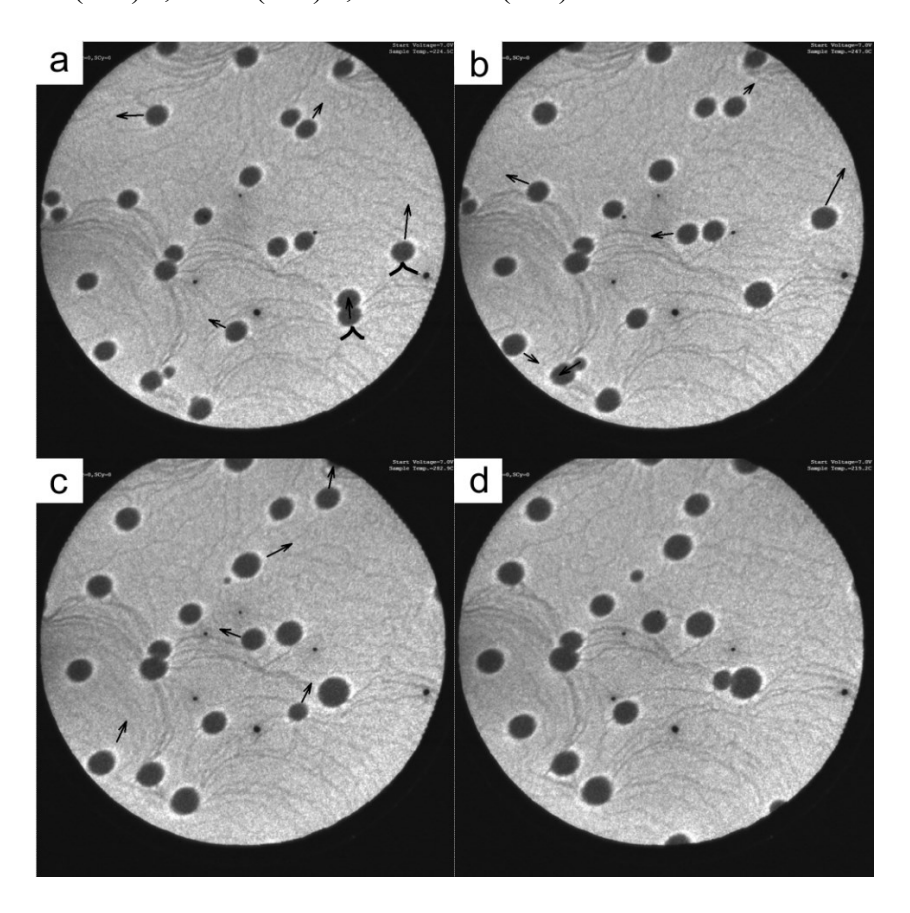


Fig.15. FOV 5 μ m. A sequence of video frames (a-d) that show the motion of some of the Au-Ge alloy droplets on the surface taken during Au dosing (as evidenced by the increasing island sizes) at ~430°C. The arrows in the images indicate the directions in which the Au-Ge alloy droplets move in the next frame. Each frame is 3 min. 20 sec. apart to show multiple islands moving, but each island moves in only ~1 second. Two black lines in (a) show kinks in the steps that point in the direction of motion of the islands. Some thermal drift is evident in the images, as the temperature was slowly drifting during the deposition.

Based on the mechanism described in Ref. 35, the increasing Au coverage in Figs. 15 and 16 (which comes from the same movie as Fig. 15) causes the observed alloy droplet motion. Fig. 16 shows a sequence of images where a smaller droplet moved towards a larger droplet until it was absorbed. The time between the second and third frame when the droplet was absorbed is only one second. Based on many different experiments, no matter which droplet was moving, the smaller droplet is always absorbed into the larger one, exhibiting island coalescence, also known as Smoluchowski ripening. Also, the change in diameter of the droplet after absorbing the other is minimal, indicating that the bulk of the newly acquired material is added to the height of the 3D droplet. Note that the behavior observed for increasing Au flux in Figs. 15-16 differs from the Ostwald ripening that was observed in Fig. 6 for heating of 6.0 ML of Au that had been deposited on Ge(111) at 200°C.

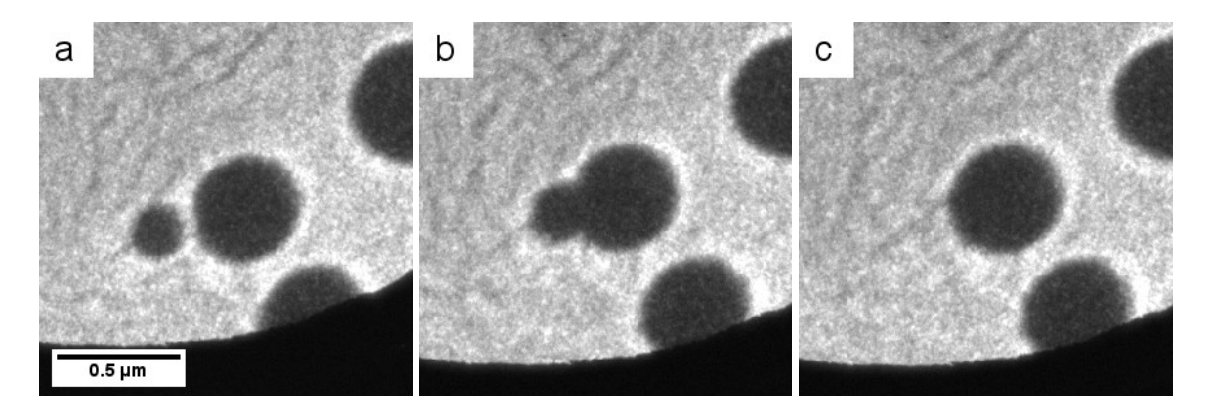


Fig. 16. A sequence of 3 frames (a-c) from a LEEM movie. A smaller Au-Ge alloy island moves towards and merges together with a larger Au-Ge alloy island. Images taken during Au deposition, with Au coverage of 10 ML at a temperature of 430°C.

We also see that surface structure and defects affect the growth of the 3D islands. Figure 17 shows a LEEM sequence of moving islands during Au dosing. Looking closely, after the first island forms and moves to join the larger island, another island begins to form from the exact spot where the first grew and from which it moved away. Then it too moves away from the

nucleation spot. This sequence replays two more times in the video data that were captured for this experiment, but the final frames are not shown here. Obviously, there is a surface defect or feature that is smaller than the resolution of the LEEM that acts as a nucleation site for the Au-Ge alloy droplets.

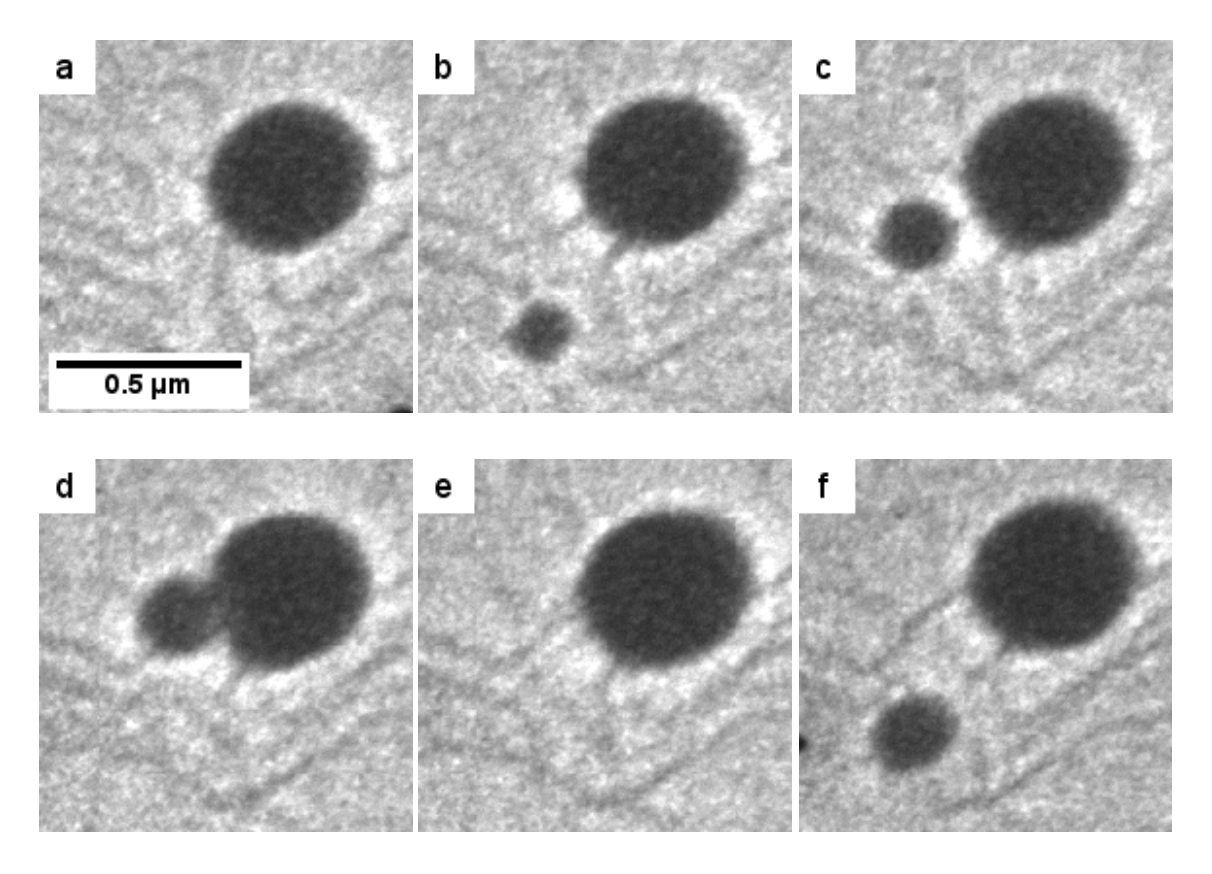


Figure 17. LEEM image sequence showing the nucleation and growth of (a) single Au-Ge alloy droplet. (b) The small island nucleates and then moves up and merges with the larger island (c-e). (f) Another Au-Ge alloy island begins to nucleate and grow from the same location as the first one in (b). Although not shown here, this process repeated another two times. These images were taken at a temperature of 430°C with Au coverage ranging from 6.2 to 7.7 ML over 496 seconds.

4. Conclusions

Au on Ge(111) thus has distinct features that differentiate it from other metal on semiconductor systems. Au thin film growth occurs via a Stranski-Krastanov mode, with one $\sqrt{3}$ layer followed by 3D Au-Ge alloy droplets forming on the surface. At temperatures above 300°C, additional Au coverage can cause an island to approach a step, where Ge dissolves into

the alloy droplet, and the resulting concentration gradient causes the hopping motion of the islands, which is accompanied by changes in the underlying step structure of the Ge substrate. This mechanism for the hopping was previously described. 35, 38, 62, 63

The Au/Ge(111) $\sqrt{3} \leftrightarrow (1x1)$ phase transition was determined to be first order from LEEM images and occurs gradually through a coexistence region with a temperature range of about 2°C. Samples with a full monolayer of Au undergo the transition at 640°C, but the transition temperature decreases to 580°C at 0.50 ML. By measuring the change in phase area during the transition of a lower coverage Au dosed sample, the coverage of the (1x1) domain was determined to be 0.37 ML.

We have discovered a unique phase transition mechanism where domains can switch back and forth between the $\sqrt{3}$ and the (1x1) phase while in the coexistence region. These domain phase fluctuations are limited to domains on the order of 12000 nm² in size. From the time dependence of the domain intensity, it is clear that the domains switch between two clearly defined phases, confirming that the transition is first order. For low step density samples with large domains, the phase fluctuations manifest themselves as boundary fluctuations, resulting in domains alternately shrinking and growing. This has the effect of giving the phase boundaries a liquid-like appearance as they fluctuate in the coexistence region. The large coverage difference between the $\sqrt{3}$ and the (1x1) means that the fluctuations cannot be thermally driven, but a surface soft phonon mode is suggested as a plausible explanation.

Supplementary Material

See supplementary material for three LEEM movies. Movie S1 is associated with Fig. 11. Movie S2 is associated with Fig. 14. Movie S3 is associated with Fig. 15.

Dedication

This paper is dedicated to Professor Patricia A Thiel, who was a brilliant experimental surface chemist, extraordinary educator, and compassionate person. Her help with the last stages of the Ph.D. dissertation of the senior author (SC) and long friendship over nearly 40 years are gratefully acknowledged.

Acknowledgements

We acknowledge partial funding support for this work from the National Science Foundation under grants CHE-0719504 and DMR-1710748. We thank T. S. Rahman and M.C. Tringides for useful discussions about the possible mechanism for the $\sqrt{3}$ to (1x1) phase transition.

Data Availability Statement

The data that support the findings of this study are available from the corresponding author upon reasonable request.

References

- ¹M. Bertucci, G. Lelay, M. Manneville, and R. Kern, Surface Science **85**, 471 (1979).
- ²M. Hammar, M. Gothelid, U. O. Karlsson, and S. A. Flodstrom, Phys. Rev. B 47, 15669 (1993).
- ³H. Huang, H. Over, S. Y. Tong, J. Quinn, and F. Jona, Phys. Rev. B 49, 13483 (1994).
- ⁴T. Takahashi and S. Nakatani, Surface Science **282**, 17 (1993).
- ⁵G. Lelay, et al., Surface Science **309**, 280 (1994).
- ⁶G. Lelay, Surface Science **132**, 169 (1983).
- ⁷G. Lelay, G. Quentel, J. P. Faurie, and A. Masson, Thin Solid Films **35**, 273 (1976).
- ⁸G. Lelay, G. Quentel, J. P. Faurie, and A. Masson, Thin Solid Films **35**, 289 (1976).
- ⁹P. B. Howes, C. Norris, M. S. Finney, E. Vlieg, and R. G. Vansilfhout, Physical Review B **48**, 1632 (1993).
- ¹⁰L. Seehofer and R. L. Johnson, Surface Science **318**, 21 (1994).
- ¹¹R. Plass and L. D. Marks, Surface Science **380**, 497 (1997).
- ¹²J. Nogami, A. A. Baski, and C. F. Quate, Physical Review Letters **65**, 1611 (1990).
- ¹³K. J. Wan, X. F. Lin, and J. Nogami, Physical Review B **45**, 9509 (1992).
- ¹⁴M. Gothelid, M. Hammar, M. Bjorkqvist, U. O. Karlsson, S. A. Flodstrom, C. Wigren, and G. Lelay, Physical Review B **50**, 4470 (1994).
- ¹⁵E. J. Vanloenen, J. E. Demuth, R. M. Tromp, and R. J. Hamers, Physical Review Letters **58**, 373 (1987).
- ¹⁶R. J. Wilson and S. Chiang, Physical Review Letters **59**, 2329 (1987).
- ¹⁷R. J. Wilson and S. Chiang, Phys. Rev. Lett. **58**, 369 (1987).
- ¹⁸D. Dornisch, W. Moritz, H. Schulz, R. Feidenhansl, M. Nielsen, F. Grey, and R. L. Johnson, Physical Review B **44**, 11221 (1991).
- ¹⁹B. J. Knapp, J. C. Hansen, M. K. Wagner, W. D. Clendening, and J. G. Tobin, Physical Review B **40**, 2814 (1989).
- ²⁰T. Takahashi, S. Nakatani, N. Okamoto, T. Ishikawa, and S. Kikuta, Japanese Journal of Applied Physics Part 2-Letters **27**, L753 (1988).
- ²¹E. Vlieg, A. W. D. Vandergon, J. F. Vanderveen, J. E. Macdonald, and C. Norris, Surface Science **209**, 100 (1989).
- ²²T. Takahashi, S. Nakatani, N. Okamoto, T. Ishikawa, and S. Kikuta, (Elsevier Science Bv, 1991), p. 54.
- ²³M. Gothelid, M. Hammar, U. O. Karlsson, C. Wigren, and G. Lelay, Phys. Rev. B **52**, 14104 (1995).
- ²⁴Y. G. Ding, C. T. Chan, and K. M. Ho, Surface Science **275**, L691 (1992).
- ²⁵H. Over, C. P. Wang, and F. Jona, Phys. Rev. B **51**, 4231 (1995).
- ²⁶C. L. H. Devlin, D. N. Futaba, A. Loui, J. D. Shine, and S. Chiang, Mat Sci Eng B-Solid **96**, 215 (2002).
- ²⁷R. J. Phaneuf and M. B. Webb, Surface Science **164**, 167 (1985).
- ²⁸Kan Nakatsuji, Yuya Motomura, Ryota Niikura, and Fumio Komori, Journal of Physics: Condensed Matter **25**, 045007 (2012).
- ²⁹J. A. Venables, J. Derrien, and A. P. Janssen, Surface Science **95**, 411 (1980).
- ³⁰G. Lelay, M. Manneville, and J. J. Metois, Surface Science **123**, 117 (1982).
- ³¹B. J. Knapp and J. G. Tobin, Physical Review B **37**, 8656 (1988).
- ³²W. C. Fan and A. Ignatiev, Physical Review B **40**, 5479 (1989).
- ³³J. A. Venables, G. D. T. Spiller, and M. Hanbucken, Rep. Prog. Phys. 47, 399 (1984).

- ³⁴W. Swiech, E. Bauer, and M. Mundschau, Surface Science **253**, 283 (1991).
- ³⁵S. Curiotto, F. Leroy, F. Cheynis, and P. Muller, Surf. Sci. **632**, 1 (2015).
- ³⁶S. Hajjar, et al., Physical Review B **84**, 125325 (2011).
- ³⁷S. Kodambaka, J. Tersoff, M. C. Reuter, and F. M. Ross, Science **316**, 729 (2007).
- ³⁸Ali El-Barraj, Stefano Curiotto, Fabien Cheynis, Pierre Müller, and Frédéric Leroy, Applied Surface Science **509**, 144667 (2020).
- ³⁹J. B. Hannon and R. M. Tromp, Ann. Rev. Mater. Res. **33**, 263 (2003).
- ⁴⁰R. J. Phaneuf and A. K. Schmid, Phys. Today **56**, 50 (2003).
- ⁴¹W. Telieps and E. Bauer, Surf. Sci. **162**, 163 (1985).
- ⁴²W. Telieps and E. Bauer, Ber. Bunsen-Ges. Phys. Chem. Chem. Phys. **90**, 197 (1986).
- ⁴³J. A. Giacomo, Ph.D. dissertation in Physics, University of California, (2009).
- ⁴⁴Caroline A. Schneider, Wayne S. Rasband, and Kevin W. Eliceiri, Nature Methods **9**, 671 (2012).
- ⁴⁵J. Canny, IEEE Trans. Pattern Anal. Mach. Intell. **8**, 679 (1986).
- ⁴⁶J. Meijering, FeatureJ, http://www.imagescience.org/meijering/software/featurej/
- ⁴⁷Y. Sato, S. Chiang, and N. C. Bartelt, Physical Review Letters **99** (2007).
- ⁴⁸Y. Sato and S. Chiang, Surface Science **603**, 2300 (2009).
- ⁴⁹Y. Sato and S. Chiang, Journal of Vacuum Science & Technology A **35**, 061405 (2017).
- ⁵⁰G. Venkataraman, Bull. Mater. Sci **1**, 129 (1979).
- ⁵¹Joseph M. Carpinelli, Hanno H. Weitering, E. Ward Plummer, and Roland Stumpf, Nature **381**, 398 (1996).
- ⁵²J. Avila, A. Mascaraque, E. G. Michel, and M. C. Asensio, Applied Surface Science **123-124**, 626 (1998).
- ⁵³Rubén Pérez, José Ortega, and Fernando Flores, Physical Review Letters **86**, 4891 (2001).
- ⁵⁴José Ortega, Rubén Pérez, and Fernando Flores, Journal of Physics: Condensed Matter 14, 5979 (2002).
- ⁵⁵C. González, F. Flores, and J. Ortega, Physical Review Letters **96**, 136101 (2006).
- ⁵⁶Talat S. Rahman, John E. Black, and Zeng Ju Tian, MRS Proceedings **291**, 205 (1992).
- ⁵⁷John E. Black, Zeng-Ju Tian, and Talat S. Rahman, Surface Science **291**, 215 (1993).
- ⁵⁸Talat S. Rahman and John E. Black, Physical Review B **48**, 5530 (1993).
- ⁵⁹P. Höpfner, et al., Physical Review B **83**, 235435 (2011).
- ⁶⁰J. B. Hannon, F. J. Meyer zu Heringdorf, J. Tersoff, and R. M. Tromp, Physical Review Letters **86**, 4871 (2001).
- ⁶¹R. M. Feenstra, A. J. Slavin, G. A. Held, and M. A. Lutz, Physical Review Letters **66**, 3257 (1991).
- ⁶²Stefano Curiotto, Frédéric Leroy, Fabien Cheynis, and Pierre Müller, Scientific Reports 7, 902 (2017).
- ⁶³F. Leroy, A. El Barraj, F. Cheynis, P. Müller, and S. Curiotto, Physical Review Letters **123**, 176101 (2019).
- ⁶⁴W. C. Yang, H. Ade, and R. J. Nemanich, Phys. Rev. B **69** (2004).
- ⁶⁵P. Bampoulis, L. Zhang, A. Safaei, R. van Gastel, B. Poelsema, and H. J. Zandvliet, J Phys Condens Matter **26**, 442001 (2014).
- ⁶⁶S. Curiotto, F. Leroy, F. Cheynis, and P. Muller, Nano Letters 15, 4788 (2015).
- ⁶⁷B. H. Stenger, A. L. Dorsett, J. H. Miller, E. M. Russell, C. A. Gabris, and S. Chiang, Ultramicroscopy **183**, 72 (2017).